Miner Petrol (2017) 111:887–908
DOI 10.1007/s00710-017-0501-7

ORIGINAL PAPER

Petrogenesis of Luchuba and Wuchaba granitoids in western Qinling: geochronological and geochemical evidence

Juanjuan Kong[1,2,3] · **Yaoling Niu**[1,2,4] · **Meng Duan**[5] · **Yu Zhang**[6] · **Yan Hu**[1] · **Jiyong Li**[1,2,3] · **Shuo Chen**[1,2,3]

Received: 25 March 2016 / Accepted: 14 February 2017 / Published online: 8 March 2017

Abstract The West Qinling Orogenic Belt (WQOB) is a major portion of the Qinling-Dabie-Sulu Orogen and holds essential information for understanding the prolonged evolution of the northeastern branch of the Paleo-Tethys in East Asia. This study focuses on the petrogenesis of granitoids from Luchuba and Wuchaba plutons in the WQOB. We obtained zircon U-Pb ages of 211 ± 1.4 Ma for the Luchuba pluton and 218.7 ± 1.3 Ma for the Wuchaba pluton, which are the same as the proposed timing of continental collision at ~220 Ma. We thus interpret the granitoids to represent a magmatic response to the collision between the North China Craton (NCC) and the Yangtze Block (YB). The two plutons are metaluminous to weakly peraluminous I-type granitoids. Samples from the two plutons show strong light rare earth element (REEs) enrichment and weak heavy REE depletion, with varying negative Eu anomalies, which is most consistent with significant plagioclase fractionation although the possible effect of plagioclase as residual phase in the magma source region cannot be ruled out. In primitive mantle normalized multi-element variation diagrams, nearly all the samples show negative Nb, Ta, P and Ti anomalies and relative enrichment in Rb, Pb, U and K. These characteristics resemble those of the average continental crust. The Luchuba pluton has lower $(^{87}Sr/^{86}Sr)_i$ (0.7051 to 0.7104), higher $\varepsilon_{Nd}(t)$ (−8.11 to −5.73) and $\varepsilon_{Hf}(t)$ (−6.70 to −1.65) than mature continental crust ($[^{87}Sr/^{86}Sr]_i > 0.72$, $\varepsilon_{Nd}(t) < -12$). The Wuchaba pluton also has lower $(^{87}Sr/^{86}Sr)_i$ (0.7069 to 0.7080), higher $\varepsilon_{Nd}(t)$ (−9.86 to −3.34) and $\varepsilon_{Hf}(t)$ (−5.69 to 1.58) than mature continental crust. We conclude that the Luchuba and Wuchaba granitoids in the WQOB are best explained as resulting from fractional crystallization with crustal assimilation of parental magmas derived from melting of Mianlue oceanic crust under amphibolite facies conditions during the initial stage of continental collision between the North China Craton and the Yangtze Block. Mafic magmatic enclaves (MMEs) of Wuchaba pluton are earlier cumulates of the same magmatic system. The Mianlue oceanic crust (MORB-like) contributes to the source of the Luchuba and Wuchaba granitoids, pointing to the significance of melting of oceanic crust for continental crust accretion.

Keywords Western Qinling · Luchuba and Wuchaba granitoids · granitoid petrogenesis · crust accretion

Introduction

The Qinling Orogen is one of the largest orogenic belts in Asia (Mattauer et al. 1985), linking Kunlun and Qilian orogens to the west and Dabie–Sulu orogen to the east (Meng and Zhang 2000; Ratschbacher et al. 2003), across Central China for ~2500 km. It developed through a series of complex seafloor

---

Editorial handling: Y. Xu

✉ Juanjuan Kong
juanjuan0317@foxmail.com

✉ Yaoling Niu
yaoling.niu@foxmail.com

[1] Institute of Oceanology, Chinese Academy of Sciences, No. 7 Nanhai Road, Shinan District, Qingdao 266071, China

[2] Laboratory for Marine Geology, Qingdao National Laboratory for Marine Science and Technology, Qingdao 266061, China

[3] University of Chinese Academy of Sciences, Beijing 100049, China

[4] Department of Earth Sciences, Durham University, Durham DH1 3LE, UK

[5] School of Earth Science and Resources, China University of Geosciences, Beijing 100083, China

[6] School of Earth Sciences, Lanzhou University, Lanzhou 730000, China

subduction and terrane collision events (Zhang et al. 2001; Ratschbacher et al. 2003; Wang et al. 2009; Wu and Zheng 2012), ultimately completed as the result of the continental collision between the Yangtze Block (YB) and the North China Craton (NCC) along the Mianlue suture zone in the early Mesozoic (see Fig. 1; Dong et al. 2011 and references therein). Abundant granitoids throughout much of the West Qinling were produced during this time period and have received much attention in recent years with mounting geochronological and geochemical data with the aim of better understanding magma sources and processes in the context of studying the Qinling orogenesis. However, the petrogenesis of these granitoids remains controversial (Sun et al. 2002a, b; Wang et al. 2007, 2011; Qin et al. 2009, 2010; Liu et al. 2011a, b; Dong et al. 2011, 2012; Yang et al. 2011, 2012; Xiao et al. 2013), and the debate mainly centers on the sources of these granitoids (e.g., upper crust, lower crust or crust-mantle magma mixing) and the geodynamic evolution.

In this paper, we focus on the Luchuba and Wuchaba granitoid plutons in the central West Qinling Orogenic Belt (WQOB) because of the geological information available due to the associated mineralization and its exploration. Existing models on the petrogenesis of these plutons include: (1) upper crust melting (Ou et al. 2010; Peng 2012, 2013); (2) lower crust melting (Xu et al. 2013); (3) partial melting of Mesoproterozoic crustal rocks and melt interaction with subcontinental lithospheric mantle (SCLM) (the interpreted source of MMEs) (Zhu et al. 2013). The crystallization age of the Wuchaba pluton has been hotly debated to vary from 264 to 213 Ma (Gao, 2011; Li et al. 2012; Peng 2012, 2013; Xu et al. 2014; Zeng et al. 2014; Wang et al. 2015) for multistage magmatic emplacement with views on tectonic settings varying from subduction-related, syn-collisional to post-collisional (Lu et al. 2004; Li et al. 2012). Debates on the petrogenesis and tectonic settings of the Luchuba and Wuchaba granitoids continued. It should be noted that previous studies on the Luchuba and Wuchaba plutons are limited with little systemic chronology, geochemistry and isotopic data. Here we present new LA-ICP-MS zircon U-Pb ages, bulk-rock major and trace element data and Sr–Nd–Hf isotopic compositions to discuss the petrogenesis of these two granitoid plutons in the context of geodynamic evolution.

Geological setting and samples

The Qinling orogenic belt is adjacent to the Qilian orogenic belt (Fig. 1a) and is bounded by the Linxia–Wushan–Tianshui fault to the north and the Mianlue suture in the south (Fig. 1b). The Qinling orogen has been divided into East and West Qinling on the basis of their geological differences (Zhang et al. 2001, 2005, 2007; Feng et al. 2002) (Fig. 1b). The granitoids with ages of 245–200 Ma are distributed between the Shangdan and Mianlue sutures along an approximately E-W trending zone (Zhu et al. 2011; Dong et al. 2011). The WQOB is interpreted as having undergone supercontinent breakup, Qinling-Qilian-Kunlun seafloor spreading and subduction, continent-continent collision and intraplate processes since the Neoproterozoic (Xu et al. 2014).

In the WQOB, the Phanerozoic strata are mostly Devonian-Cretaceous sedimentary units with minor Cambrian-Silurian sedimentary units. The Precambrian basement is rarely exposed (Feng et al. 2002). Zhang et al. (2007) confirm that the basement of the WQOB has affinities with the Yangtze block. The Luchuba pluton crops out over an area of ~117 km^2, intruding Devonian and Carboniferous limestone, sandstone and shale (Ou et al. 2010). The Wuchaba pluton, also known as Zhongchuan pluton, has a circular shape with an outcrop area of ~210 km^2 (Zeng et al. 2012), intruding the Middle Devonian Shujiaba group (D2sh^1) and Carboniferous Xiajialing group (C1x) (Fig. 1c). In the field, the Luchuba granitoids are light grey, and structurally massive with medium-grained or porphyritic texture (Fig. 2a). The Wuchaba granitoids (Fig. 2b) are light red and smoky gray in color, with medium-to coarse-grained and porphyritic texture. Mafic magmatic enclaves (MMEs) occur locally in both Luchuba and Wuchaba plutons, exhibit angular to oval shapes and varying size (10 to 20 cm in diameter), and have no chilled margins with the host granitoids (Fig. 2a, b).

The Luchuba granitoids are mainly composed of granodiorite (Fig. 3a) and biotite monzogranite (Fig. 3b), and have porphyritic texture with the mineral assemblage of plagioclase (~30 to 40%) + K-feldspar (~10 to 20%) + quartz (~30 to 40%) with total biotite + hornblende (~5 to 10%). The Wuchaba pluton mainly includes biotite monzogranite (Fig. 3c), biotite granite and diorite with the mineral assemblage similar to that of the Luchuba pluton. The mineralogy is dominantly plagioclase (~30%), quartz (~20%), K-feldspar (~30 to 40%) with minor hornblende and biotite (~10% in total) and accessory minerals such as apatite, zircon and Fe-Ti oxides. The MMEs are fine-grained and show equigranular and hypidiomorphic textures. It is important to note that the MMEs share the same mineralogy with the more felsic hosts but have greater modes of mafic minerals (~55% hornblende and biotite) and lesser plagioclase (~20%), quartz (~10%) and K-feldspar (~10%) (Fig. 3d,e). Acicular apatite is ubiquitous in the MMEs (Fig. 3f). Euhedral to subhedral plagioclase crystals

Fig. 1 **a**, **b** Simplified geological map of the western Qinling Orogenic belt (modified from Zhang et al. 2007). In **c** I = fine grained porphyritic tourmaline-bearing biotite monzonitic granite; II = fine grained porphyritic biotite monzonitic granite; III = medium-fine grained biotite monzonitic granite; IV = medium-fine grained granodiorite; V = medium grained biotite monzonitic granite; VI = porphyritic biotite monzonitic granite; VII = porphyritic monzonitic granite; and VIII = medium to fine grained biotite monzonitic granite. ▶

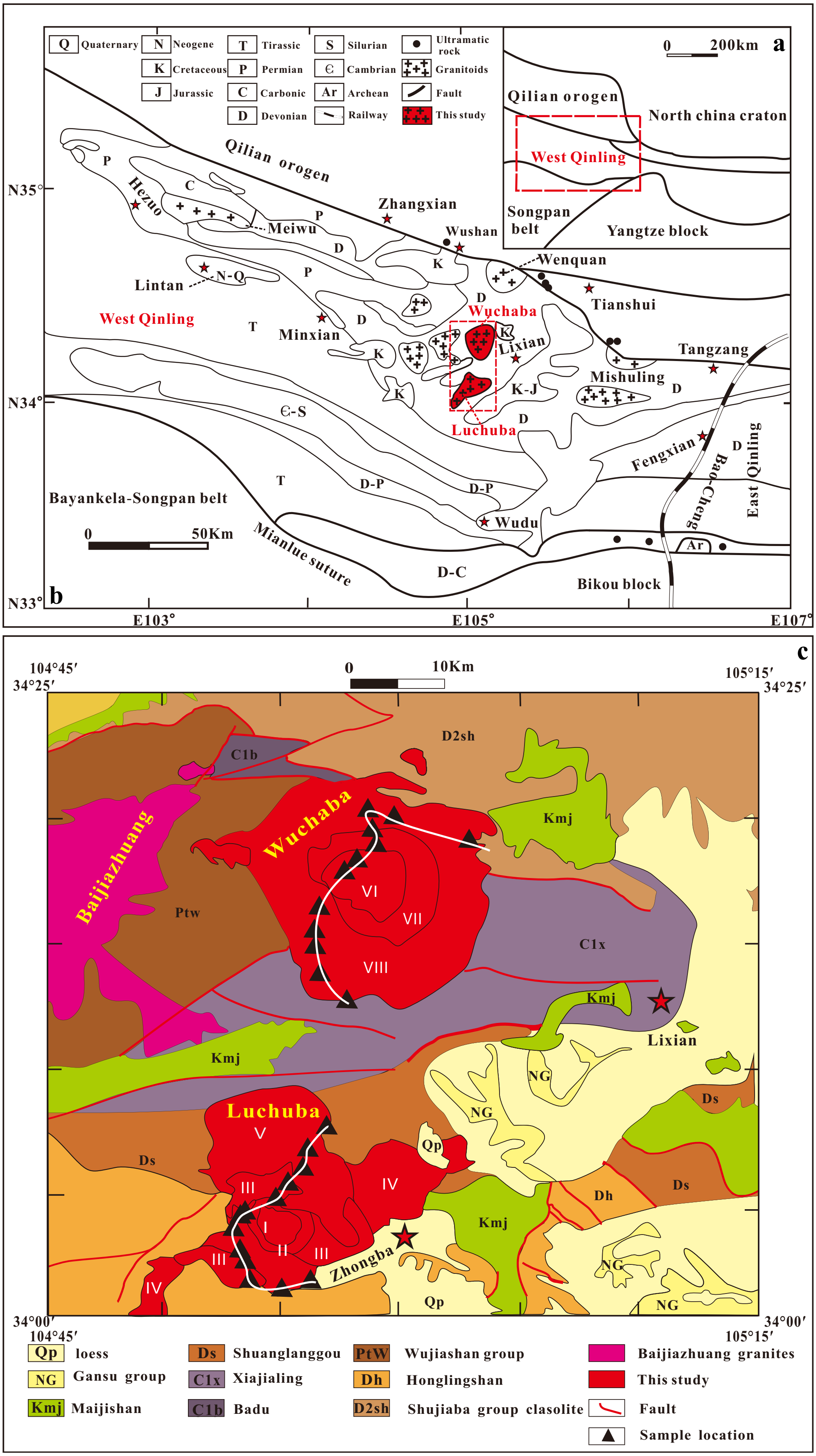
a
0 200km
Qilian orogen
North china craton
West Qinling
Songpan belt
Yangtze block
Q Quaternary
N Neogene
K Cretaceous
J Jurassic
T Tirassic
P Permian
C Carbonic
D Devonian
S Silurian
Є Cambrian
Ar Archean
Railway
Ultramatic rock
Granitoids
Fault
This study
b
N35°
N34°
N33°
E103°
E105°
E107°
Qilian orogen
Hezuo
Meiwu
Zhangxian
Wushan
Wenquan
Tianshui
Lintan
N-Q
West Qinling
Minxian
Wuchaba
Lixian
Luchuba
Tangzang
Mishuling
K-J
Fengxian
Bao-Cheng
East Qinling
Є-S
D-P
Bayankela-Songpan belt
0 50Km
Mianlue suture
Wudu
D-C
Bikou block
Ar
P
C
D
T
K
c
104°45′
34°25′
0 10Km
105°15′
34°25′
D2sh
C1b
Wuchaba
Baijiazhuang
Ptw
Kmj
VI
VII
VIII
C1x
Kmj
Lixian
NG
Ds
Luchuba
V
Qp
IV
III
I
II
III
Zhongba
Dh
34°00′
104°45′
105°15′
34°00′
Qp loess
NG Gansu group
Kmj Maijishan
Ds Shuanglanggou
C1x Xiajialing
C1b Badu
PtW Wujiashan group
Dh Honglingshan
D2sh Shujiaba group clasolite
Baijiazhuang granites
This study
Fault
Sample location

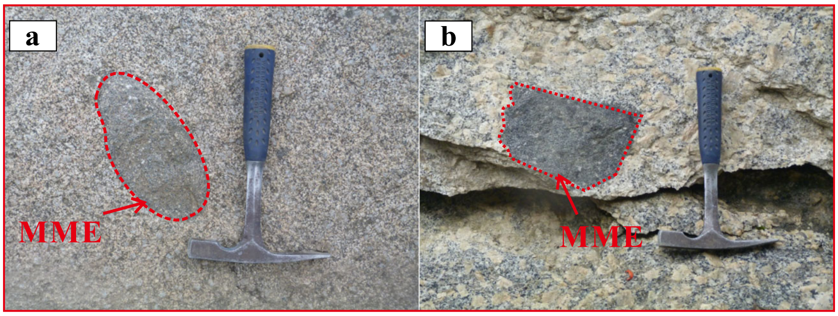

Fig. 2 **a** Outcrop of Luchuba granitoid pluton with mafic magmatic enclaves (MMEs). **b** Outcrop of Wuchaba granitoid pluton with MMEs

occur either as phenocrysts or as elongate laths. Quartz commonly occurs as anhedral grains. K-feldspar is mainly megacrysts. Apatite and hornblende display euhedral habit.

Analytical methods

In this study, 24 representative samples (including 2 host-MME pairs) from the Luchuba and Wuchaba plutons were analyzed for whole-rock major and trace elements, three of these representative samples were selected for zircon U-Pb dating. Fifteen of these samples were analyzed for whole-rock Sr-Nd-Hf isotope compositions. Weathered surfaces were removed and thoroughly cleaned, then ultrasonically cleaned with Milli-Q water and dried before the material was powdered to less than 200-mesh in a clean environment using an agate mill for analysis.

LA-ICP-MS zircon U–Pb dating

Zircons were extracted using combined techniques of heavy liquid and magnetic separation. The zircon internal structure was examined using cathodoluminescence (CL) imaging on an EMPA-JXA-8100 scanning electron microscope at China

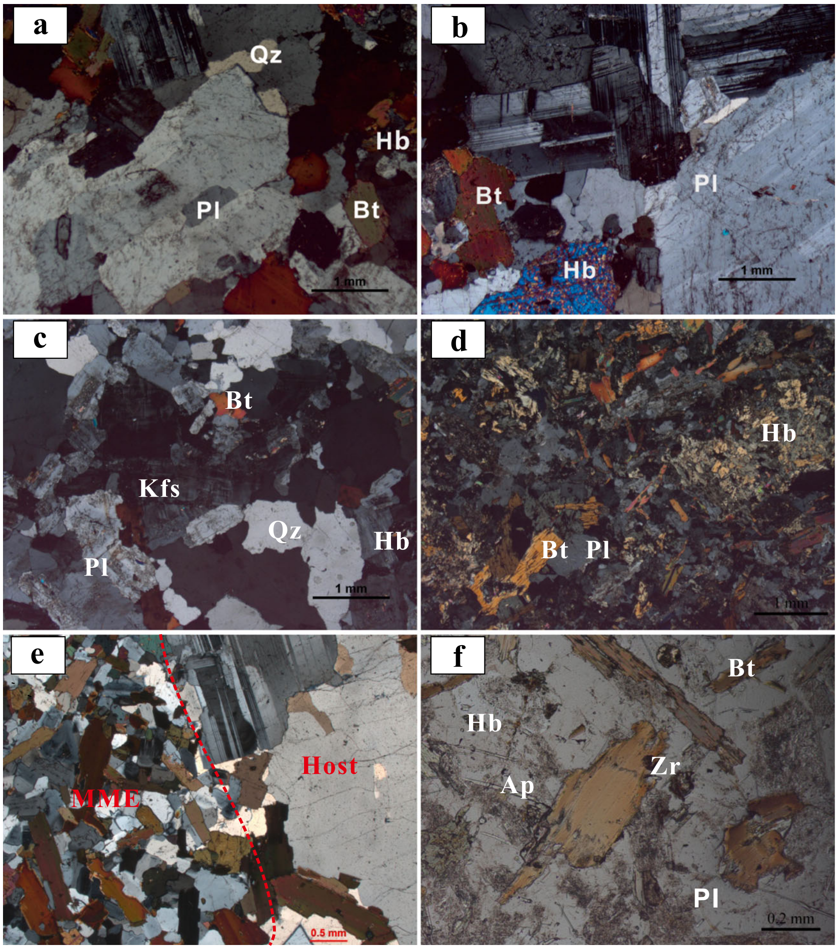

Fig. 3 Photomicrographs of Luchuba and Wuchaba plutons. **(a)** Sample SEB12–01 and **(b)** Sample YDB12–05 of Luchuba (cross-polarized light or XPL) pluton; **(c)** Sample DPC12–01 and **(d)** Sample MK12–04 of Wuchaba (XPL) pluton. **(e)** showing the sharp contact of MMEs with their host granodiorite, and MMEs are finer-grained than the host. **(f)** Sample MK12–04 of Wuchaba (PPL) pluton. The abbreviations are as follows: Pl - plagioclase, Qz - quartz, Bt - biotite, Hb - hornblende, Kfs - K-feldspar, Ap - apatite, Zr - zircon

University of Geosciences, Wuhan (CUGW) (Fig. 4). Zircon U-Pb dating on samples SEB12–01, YDB12–05 and DPC12–01 was carried out at the Geologic Lab Center, China University of Geosciences, Beijing (CUGB) using an Agilent 7500a inductively coupled plasma mass spectrometer (ICP-MS) with New Wave UPP-193 laser ablation system. During the analysis, laser spot size was set to ~36 μm for most analyses and to 25 μm for metamorphic rims with laser energy density set at 8.5 J/cm^2 and repetition rate at 10 Hz. The procedure of laser sampling is 5 s pre-ablation, 20s sample-chamber flushing and 40s sampling ablation. The ablated material is carried into the ICP-MS by the high-purity Helium gas stream with a flux of 0.8 L/min. The whole laser path was fluxed with N_2 (15 L/min) and Ar (1.15 L/min) in order to increase energy stability. The counting time for U, Th, ^{204}Pb, ^{206}Pb, ^{207}Pb and ^{208}Pb is 20 ms, and is 15 ms for other elements. Calibrations for the zircon analyses were carried out using NIST 610 as an external standard and Si as internal standard. U-Pb isotope fractionation effects were corrected for using zircon 91,500 (Wiedenbeck et al. 1995) as external standard. The data were processed using the GLITTER4.41 program with common Pb correction done following Andersen (2002) and analytical details described in Song et al. (2010a). The age data are given in Table 2 and the concordia diagrams and weighted mean age calculations were done using ISOPLOT 4.15 (Ludwig 2012; Fig. 5).

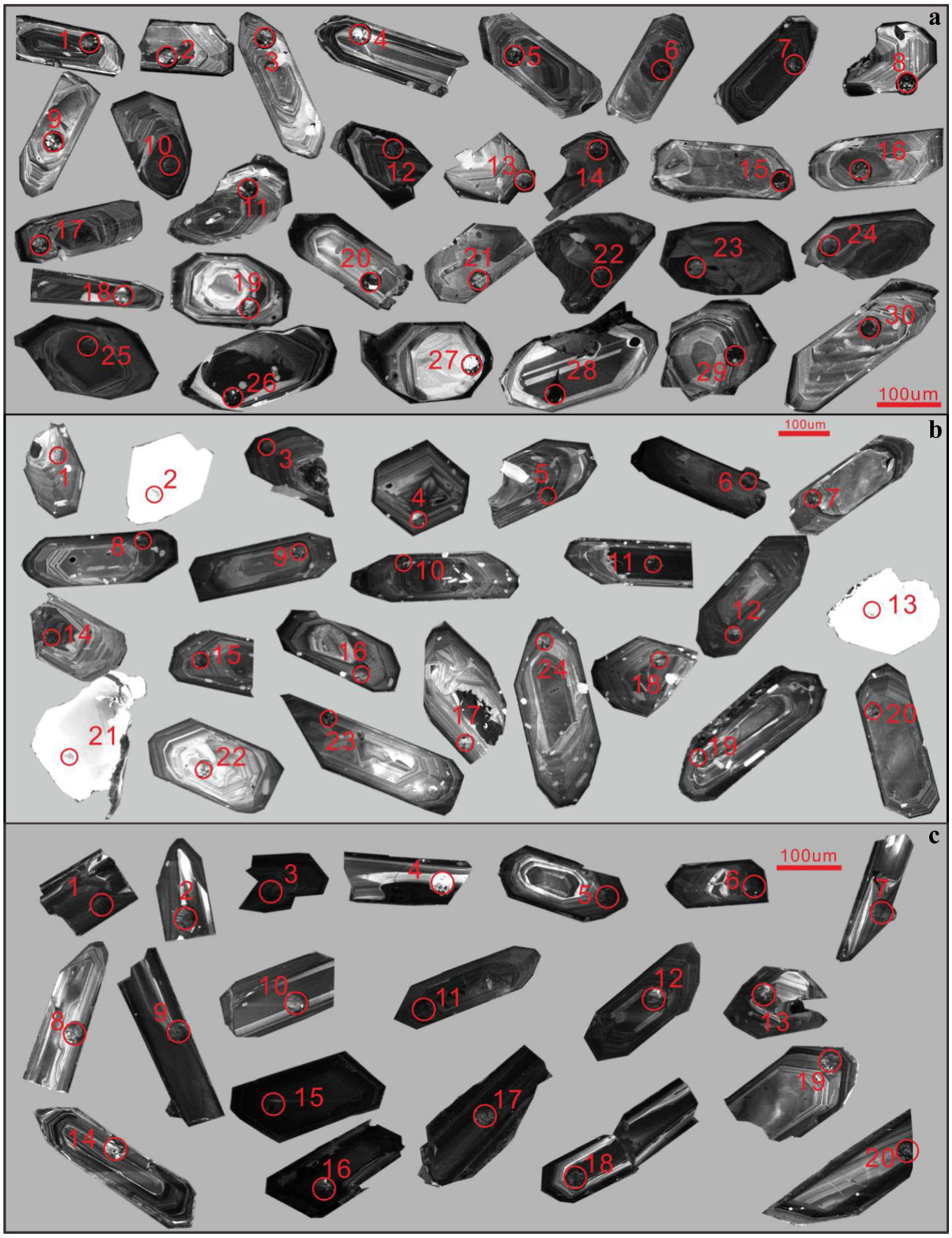

Fig. 4 Cathodoluminescence (CL) images of zircons from representative samples **(a)** SEB12–01 and **(b)** YDB12–05 of Luchuba pluton; **(c)** DPC12–01 of Wuchaba pluton. Red circles show analyzed spots

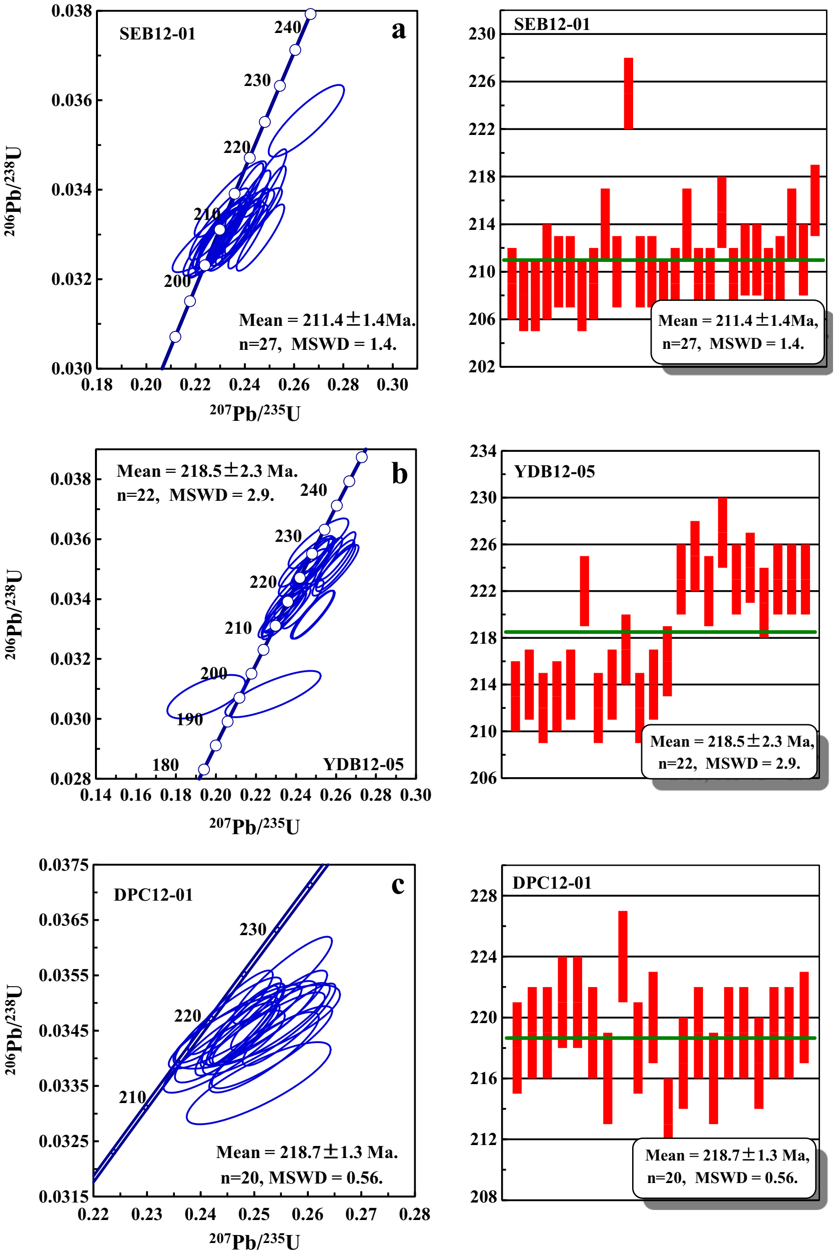

Fig. 5 Zircon U–Pb concordia plots and weighted mean $^{206}Pb/^{238}U$ ages for **(a)** SEB12–01 and **(b)** YDB12–05 of Luchuba pluton, and ***(c)*** DPC12–01 of Wuchaba pluton

Major and trace elements

Whole-rock major and trace elements were analyzed using Prodigy Inductively Coupled Plasma Optical Emission Spectrometer (ICP-OES) and Agilent 7500a ICP-MS, respectively at CUGB. Analyses of United States Geological Survey (USGS) rock standards (AGV-2 and GSR-1) and Chinese national rock standard (GSR-3) give precision and accuracy better than 5% (2σ) for major elements and 10% (2σ) for trace elements. Analytical details are given in Song et al. (2010b).

Sr–Nd–Hf isotopes

For Sr, Nd and Hf isotope analyses, about 100 mg of sample powder was dissolved in a HF + HNO_3 mixture in Teflon beakers. The Sr, Nd and Hf were then separated using cation-exchange techniques. The Sr isotope reatios were measured using a Finnigan Triton Thermal Ionization Mass Spectrometer (TIMS) and the Hf and Nd isotope ratios were measured using Multi-Collector Inductively Coupled Plasma Mass Spectrometry (MC-ICP-MS) at Guangzhou Institute of

Geochemistry. The $^{87}Sr/^{86}Sr$, $^{143}Nd/^{144}Nd$ and $^{176}Hf/^{177}Hf$ ratios are reported as values normalized to $^{86}Sr/^{88}Sr$ of 0.1194, $^{146}Nd/^{144}Nd$ of 0.7219 and $^{179}Hf/^{177}Hf$ of 0.7325, respectively. During our analysis, repeated analyses of the NBS-987 Sr standard yielded $^{87}Sr/^{86}Sr = 0.710287 \pm 20$ ($n = 21$, 2σ) and JNdi-1 Nd standard gave $^{143}Nd/^{144}Nd$ 0.512086 ± 16 ($n = 11$, 2σ). Analyses of Hf standard yielded $^{176}Hf/^{177}Hf$ of 0.283099 ± 15 ($n = 13$, 2σ) for BHVO-2 and 0.283216 ± 15 ($n = 6$, 2σ) for JB-3, which are consistent with the reference values (Raczek et al. 2003, Li et al. 2010). Sample preparation procedures and analytical details are described in Wei et al. (2002) and Li et al. (2004, 2005).

Results

Zircon U–Pb data

Zircon cathodoluminescence (CL) images are shown in Fig. 4. Most zircons are euhedral with oscillatory or linear zoning, ranging from 100 to 300 μm in length with variable Th (65 to 805 ppm), U (175 to 3300 ppm) and Th/U ratio (0.058 to 1.04), which is consistent with a magmatic origin (Rubatto and Gebauer 2000; Corfu et al. 2003; Hanchar and Hoskin 2003; Cao et al. 2011).

Thirty grains of zircon from sample SEB12–01 of the Luchuba pluton were analyzed (Table 1). Three spots were excluded in the age calculation because of their high ^{204}Pb and significant deviation from the concordia. Twenty-seven spots form a cluster giving a weighted mean $^{206}Pb/^{238}U$ age of 211 ± 1.4 Ma (MSWD =1.4, $n = 27$) (Fig. 5a). All the 24 zircon grains from sample YDB12–05 of the Luchuba pluton plot close to the concordia curve (Fig. 5b). Two grains give younger ages of 195 Ma and 196 Ma probably due to Pb loss. Other grains give a weighted mean $^{206}Pb/^{238}U$ age of 218.5 ± 2.3 Ma (MSWD =2.9, $n = 22$). Twenty zircons from sample DPC12–01 of the Wuchaba pluton give a weighted mean $^{206}Pb/^{238}U$ age of 218.3 ± 1.7 Ma (MSWD =0.56, $n = 20$) (Fig. 5c). All these are interpreted as crystallization ages of the two plutons. The two distinct ages of 211 ± 1.4 Ma and 218.5 ± 2.3 Ma of the Luchuba pluton suggests prolonged magmatism during the same event.

Major and trace elements

Whole-rock major and trace element compositions of the granitoids and MMEs from the Luchuba and Wuchaba plutons are given in Table 2. The Luchuba granitoids show varying SiO_2 (64.15 to 75.82 wt.%) as do the Wuchaba granitoids (64.61 to 73.91 wt.% SiO_2). In the $K_2O + Na_2O$ vs. SiO_2 diagram (Fig. 6), most of the samples from the Luchuba and Wuchaba granitoids display a roughly continuous compositional spectrum from granodiorite to granite in subalkaline field with aluminum saturation index ([ASI = molar Al_2O_3/ ($CaO + K_2O + Na_2O$)]) ≤ 1.10 (Fig. 7). They exhibit a high K character with high K_2O/Na_2O (1.02 to 1.32 for Luchuba and 1.11 to 2.28 for Wuchaba plutons, Table 3). The high K_2O sample (MZG12–02) has high modal biotite and K-feldspar (~30%), while the low K_2O sample (CJM12–01(host)) has few modal biotite and K-feldspar (< 5%). In SiO_2 variation diagrams (Fig. 8), most samples from the two plutons define a roughly correlated evolution trend: Al_2O_3, CaO, Fe_2O_3, MgO, TiO_2, P_2O_5, Sr, Eu and Yb decrease with increasing SiO_2 whereas Na_2O and K_2O increase with increasing SiO_2. The Luchuba granitoids display strongly fractionated REE patterns ($(La/Yb)_N = 5.28$ to 18.84) with moderately negative Eu anomalies (Eu/Eu* = 0.41 to 0.83) (Fig. 9a). The Wuchaba granitoids show moderate to strong LREE enrichment ($(La/Yb)_N = 4.13$ to 34.61) and variable negative Eu anomalies (Eu/Eu* = 0.16 to 0.86; Fig. 9c). Samples from the Luchuba and Wuchaba plutons have low Sr content and significant negative Sr anomalies ($Sr/Sr^* = 2Sr_N/[Pr_N + Nd_N]$), corresponding to its significant negative Eu anomalies (Fig. 10), which is most consistent with significant plagioclase fractionation although the possible effect of plagioclase as residual phase in the magma source region cannot be ruled out. In the trace element spider diagrams, all the samples show negative Nb, Ta, P and Ti anomalies and Rb, Th, U and K enrichment (Fig. 9b, d). These characteristics resemble those of bulk continental crust (BCC; Rudnick and Gao 2003).

The MMEs from the Wuchaba pluton have relatively lower SiO_2 contents (53.31 and 53.92 wt.%; Figs. 6, 7 and 8) and show the same composition in the TAS diagram (Fig. 6). The MMEs have negative Eu anomalies with Eu/Eu* of 0.26 and 0.65, displaying higher abundances of HREEs (Fig. 9c) and higher Nb/Ta (17.52 and 17.38) than the host, which is consistent with higher modal contents of hornblende (Foley et al. 2000; Niu and O'Hara 2009; Chen et al. 2015, 2016).

Sr-Nd-Hf isotopes

Whole rock Sr-Nd-Hf isotope data for 15 samples (including two MMEs) of the two plutons are given in Table 3 and plotted in Figs. 11, 12 and 13. The $I_{Sr}(t)$, $\varepsilon_{Nd}(t)$ and $\varepsilon_{Hf}(t)$ refer to the age ($t = 220$ Ma) corrected values. All the analyzed Luchuba samples have variable values of $I_{Sr}(t)$ (0.7052 to 0.7104), $\varepsilon_{Nd}(t)$ of −8.11 to −5.73 and $\varepsilon_{Hf}(t)$ of −6.70 to −1.65. The Wuchaba pluton has the

Table 1 Zircon U–Pb data for the Luchuba and Wuchaba pluton

No.	Element(ppm)			Th/U	Isotope ratio						Apparent age(Ma)					
	Pb*	U	Th		$^{207}Pb/^{206}Pb$	1	$^{207}Pb/^{235}U$	1	$^{206}Pb/^{238}U$	1	$^{207}Pb/^{206}Pb$	1	$^{207}Pb/^{235}U$	1	$^{206}Pb/^{238}U$	1
Sample SEB12–01(Luchuba Pluton)																
SEB-1	19.7	559	261	0.47	0.0543	0.0014	0.2463	0.0064	0.0329	0.0005	381	32	224	5	209	3
SEB-2	16.1	459	183	0.40	0.0505	0.0016	0.2284	0.0074	0.0328	0.0005	216	47	209	6	208	3
SEB-3	16.4	441	269	0.61	0.0502	0.0018	0.2273	0.0081	0.0329	0.0005	202	54	208	7	208	3
SEB-4	6.4	175	105	0.60	0.0507	0.0030	0.2313	0.0137	0.0331	0.0006	227	102	211	11	210	4
SEB-5	18.1	517	174	0.34	0.0507	0.0014	0.2315	0.0068	0.0331	0.0005	227	40	211	6	210	3
SEB-6	21.7	568	400	0.70	0.0518	0.0014	0.2361	0.0067	0.0330	0.0005	277	38	215	5	210	3
SEB-7	18.5	525	211	0.40	0.0503	0.0015	0.2273	0.0068	0.0328	0.0005	208	42	208	6	208	3
SEB-8	18.8	511	285	0.56	0.0507	0.0014	0.2299	0.0066	0.0329	0.0005	226	39	210	5	209	3
SEB-9	31.4	914	191	0.21	0.0520	0.0012	0.2418	0.0057	0.0337	0.0005	287	29	220	5	214	3
SEB-10	13.9	389	164	0.42	0.0587	0.0019	0.2674	0.0086	0.0330	0.0005	557	44	241	7	209	3
SEB-11	18.0	223	182	0.81	0.0547	0.0017	0.5114	0.0159	0.0677	0.0010	402	43	419	11	423	6
SEB-12	15.7	445	164	0.37	0.0506	0.0014	0.2307	0.0067	0.0331	0.0005	224	40	211	6	210	3
SEB-13	28.2	796	298	0.37	0.0523	0.0011	0.2385	0.0052	0.0331	0.0005	297	25	217	4	210	3
SEB-14	19.1	486	149	0.31	0.0541	0.0022	0.2650	0.0101	0.0355	0.0005	374	95	239	8	225	3
SEB-15	15.7	446	154	0.35	0.0508	0.0015	0.2318	0.0069	0.0331	0.0005	230	41	212	6	210	3
SEB-16	20.0	571	215	0.38	0.0507	0.0014	0.2295	0.0063	0.0328	0.0005	226	37	210	5	208	3
SEB-17	21.6	624	189	0.30	0.0515	0.0014	0.2340	0.0066	0.0330	0.0005	262	38	213	5	209	3
SEB-18	56.7	1655	281	0.17	0.0535	0.0010	0.2491	0.0050	0.0338	0.0005	348	22	226	4	214	3
SEB-19	36.4	1087	250	0.23	0.0531	0.0011	0.2412	0.0053	0.0330	0.0005	333	25	219	4	209	3
SEB-20	24.9	728	190	0.26	0.0502	0.0014	0.2283	0.0064	0.0330	0.0005	204	38	209	5	209	3
SEB-21	46.5	1336	306	0.23	0.0514	0.0010	0.2397	0.0051	0.0339	0.0005	257	25	218	4	215	3
SEB-22	22.8	625	336	0.54	0.0503	0.0014	0.2288	0.0065	0.0330	0.0005	209	39	209	5	209	3
SEB-23	15.1	423	172	0.41	0.0525	0.0021	0.2408	0.0095	0.0333	0.0005	308	61	219	8	211	3
SEB-24	42.1	1219	301	0.25	0.0524	0.0012	0.2407	0.0058	0.0333	0.0005	304	30	219	5	211	3
SEB-25	21.2	597	224	0.38	0.0520	0.0016	0.2365	0.0075	0.0330	0.0005	286	45	216	6	209	3
SEB-26	29.4	867	186	0.21	0.0521	0.0013	0.2374	0.0061	0.0331	0.0005	288	32	216	5	210	3
SEB-27	12.5	360	77	0.21	0.0502	0.0021	0.2341	0.0096	0.0338	0.0006	206	64	214	8	214	3
SEB-28	15.4	419	135	0.32	0.0501	0.0017	0.2296	0.0079	0.0332	0.0005	200	51	210	7	211	3
SEB-29	24.3	525	435	0.83	0.0980	0.0043	0.4712	0.0192	0.0349	0.0006	1586	84	392	13	221	4
SEB-30	37.1	1061	232	0.22	0.0527	0.0012	0.2481	0.0058	0.0342	0.0005	315	28	225	5	216	3
Sample YDB12–05(Luchuba pluton)																
YDB-1	24.8	719	136	0.19	0.0504	0.0015	0.2332	0.0069	0.0336	0.0005	213	40	213	6	213	3
YDB-2	31.8	897	223	0.25	0.0522	0.0015	0.2435	0.0068	0.0338	0.0005	295	36	221	6	214	3
YDB-3	29.1	836	186	0.22	0.0537	0.0015	0.2481	0.0071	0.0335	0.0005	360	37	225	6	212	3
YDB-4	12.4	353	84	0.24	0.0506	0.0019	0.2343	0.0086	0.0336	0.0006	224	55	214	7	213	3
YDB-5	25.7	725	198	0.27	0.0506	0.0015	0.2350	0.0071	0.0337	0.0005	220	41	214	6	214	3
YDB-6	29.6	800	212	0.27	0.0539	0.0016	0.2597	0.0076	0.0350	0.0006	366	38	234	6	222	3
YDB-7	26.2	747	185	0.25	0.0539	0.0015	0.2489	0.0069	0.0335	0.0005	366	35	226	6	212	3
YDB-8	31.1	879	207	0.24	0.0506	0.0015	0.2349	0.0070	0.0337	0.0005	220	40	214	6	214	3
YDB-9	31.4	771	159	0.21	0.0538	0.0038	0.2285	0.0158	0.0308	0.0005	360	164	209	13	196	3
YDB-10	28.4	787	209	0.27	0.0508	0.0015	0.2397	0.0070	0.0342	0.0005	233	39	218	6	217	3
YDB-11	27.3	782	187	0.24	0.0507	0.0016	0.2341	0.0073	0.0335	0.0005	228	43	214	6	212	3
YD B-12	45.7	1315	257	0.20	0.0502	0.0014	0.2334	0.0066	0.0337	0.0005	202	37	213	5	214	3
YDB-13	26.9	751	195	0.26	0.0502	0.0016	0.2360	0.0074	0.0341	0.0006	204	43	215	6	216	3
YDB-14	22.0	596	189	0.32	0.0504	0.0018	0.2451	0.0090	0.0353	0.0006	213	56	223	7	223	3
YDB-15	63.9	1718	805	0.47	0.0534	0.0011	0.2609	0.0059	0.0355	0.0005	344	26	235	5	225	3
DPC-16	51.8	1434	239	0.17	0.0530	0.0017	0.2532	0.0072	0.0346	0.0005	331	74	229	6	219	3
DPC-17	61.9	1732	210	0.12	0.0518	0.0016	0.2450	0.0065	0.0343	0.0005	277	70	222	5	217	3
DPC-18	50.0	1384	232	0.17	0.0529	0.0016	0.2518	0.0068	0.0345	0.0005	323	71	228	6	219	3
DPC-19	58.1	1684	176	0.10	0.0520	0.0009	0.2484	0.0048	0.0346	0.0005	287	21	225	4	219	3
DPC-20	24.9	714	78	0.11	0.0525	0.0017	0.2509	0.0070	0.0346	0.0005	309	74	227	6	220	3

Table 2 Major (wt.%) and trace element concentrations (ppm) of the Luchuba and Wuchaba pluton

	Luchuba pluton						Wuchaba pluton					
Sample	SEB12–01	SEB12–02	BSB12–01	YDB12–03	YDB12–05	NSC12–01	TJZ12–01	LTB12–01	ZKL12–01	DBQ12–01	DBQ12–03	ZTC12–01
Major elements (wt.%)												
SiO_2	65.20	64.15	66.63	66.75	67.18	71.29	69.94	70.51	75.28	69.92	70.03	68.95
TiO_2	0.60	0.59	0.50	0.55	0.50	0.28	0.30	0.31	0.05	0.35	0.40	0.38
Al_2O_3	14.98	15.66	15.74	15.04	15.28	14.64	14.91	14.53	13.78	14.90	14.29	15.38
TFe_2O_3	4.41	4.12	3.40	3.92	3.44	1.81	1.93	2.28	0.85	2.54	2.97	2.76
MnO	0.07	0.06	0.06	0.07	0.06	0.04	0.04	0.04	0.02	0.05	0.06	0.06
MgO	2.64	2.77	1.66	2.58	1.70	0.77	0.88	0.99	0.27	0.82	0.92	0.86
CaO	3.86	3.85	2.96	3.58	3.03	1.89	2.07	2.27	0.39	2.04	2.20	1.99
Na_2O	3.32	3.44	3.56	3.19	3.35	3.62	3.59	3.44	3.72	3.15	3.04	3.26
K_2O	3.51	3.52	4.61	3.89	4.39	4.35	4.39	4.28	4.91	4.96	4.12	4.84
P_2O_5	0.17	0.16	0.18	0.14	0.22	0.08	0.14	0.10	0.11	0.12	0.18	0.14
LOI	0.66	1.34	0.43	0.87	0.74	0.87	0.74	0.44	0.56	0.38	0.85	0.73
$Na_2O + K_2O$	6.83	6.96	8.17	7.08	7.74	7.96	7.97	7.73	8.63	8.11	7.16	8.10
K_2O/Na_2O	1.06	1.02	1.29	1.22	1.31	1.20	1.22	1.24	1.32	1.58	1.36	1.48
A/CNK	0.97	1.01	0.97	0.98	0.98	1.01	1.01	1.00	1.03	1.00	1.04	1.04
Total	99.43	99.66	99.75	100.58	99.90	99.63	98.92	99.20	99.93	99.24	99.08	99.36
Trace elements (ppm)												
Li	68.8	18.7	87.1	80.4	78.0	104	121	110	22.9	83.9	90.5	80.4
P	657	590	736	699	713	302	430	443	255	571	588	562
K	36,140	34,200	41,520	44,800	42,580	35,760	40,580	42,140	49,860	57,740	42,360	50,540
Sc	10.4	10.1	7.03	10.2	8.08	3.54	5.26	4.93	2.96	5.33	6.17	5.74
Ti	4368	4080	3276	4448	3558	1742	2080	2108	316	2846	2916	2722
V	85.0	76.4	54.2	80.8	62.3	25.1	66.0	31.5	3.65	32.9	33.9	31.5
Cr	109	115	46.2	103	49.8	18.0	22.1	22.3	2.89	11.1	11.5	11.4
Mn	588	441	476	574	503	289	356	336	119	491	532	499
Co	12.3	10.0	7.47	11.6	8.71	3.21	3.66	4.22	0.31	4.34	4.40	4.30
Ni	26.4	34.1	11.2	24.5	13.3	5.63	7.97	6.05	1.24	3.26	3.54	3.57
Cu	11.4	3.79	4.09	7.07	11.0	1.20	1.38	2.41	1.11	1.06	1.76	1.94
Zn	68.6	53.0	52.0	49.4	50.7	40.5	38.6	41.8	30.5	45.2	63.1	69.7
Ga	21.9	20.0	18.5	20.0	20.9	19.7	20.9	20.1	18.3	22.3	20.7	21.2
Rb	167	144	173	165	208	184	213	215	254	276	257	234
Sr	407	383	372	381	416	224	279	287	70.0	374	289	377
Y	17.3	17.7	14.9	15.7	17.1	10.9	13.5	12.8	17.0	20.1	20.8	16.1
Zr	198	190	121	173	196	121	140	122	45.9	214	194	173
Nb	16.5	15.1	14.0	14.1	15.7	14.5	16.0	14.4	11.1	20.1	22.0	17.9
Cs	12.8	8.92	9.58	12.6	13.5	15.9	18.5	15.9	20.0	15.7	21.7	14.8
Ba	874	879	815	834	875	458	559	697	270	1042	579	963
La	35.3	35.5	24.4	35.7	39.0	29.1	25.3	28.9	10.6	35.5	44.9	30.9
Ce	71.2	67.8	61.8	69.2	73.1	54.7	46.3	55.5	21.9	68.9	88.0	65.6
Pr	7.55	7.49	5.53	7.16	7.87	5.72	5.20	5.84	2.39	7.58	9.34	6.59
Nd	27.5	27.6	20.3	25.6	28.6	20.2	18.9	20.8	8.73	27.9	33.8	24.0
Sm	5.11	5.12	4.12	4.63	5.27	3.77	3.79	3.96	2.31	5.51	6.32	4.74
Eu	1.22	1.19	1.06	1.10	1.23	0.686	0.881	0.888	0.327	1.34	1.00	1.27
Gd	4.36	4.34	3.55	3.97	4.45	3.04	3.26	3.27	2.50	4.72	5.32	4.11
Tb	0.58	0.57	0.48	0.52	0.59	0.39	0.45	0.43	0.45	0.64	0.70	0.55
Dy	3.18	3.16	2.64	2.91	3.15	2.00	2.41	2.28	2.77	3.47	3.75	2.95
Ho	0.61	0.61	0.50	0.56	0.60	0.36	0.45	0.42	0.53	0.67	0.69	0.54
Er	1.77	1.78	1.39	1.63	1.66	1.00	1.26	1.22	1.54	1.94	1.99	1.55

Table 2 (continued)

Tm	0.24	0.25	0.20	0.22	0.24	0.14	0.18	0.17	0.23	0.28	0.27	0.21
Yb	1.58	1.61	1.30	1.48	1.48	0.89	1.17	1.12	1.45	1.86	1.79	1.36
Lu	0.23	0.24	0.19	0.22	0.23	0.13	0.17	0.17	0.21	0.28	0.26	0.20
Hf	4.95	4.53	3.07	4.35	4.62	3.23	3.76	3.31	1.60	5.21	4.76	4.27
Ta	1.02	0.94	0.95	1.08	0.96	0.90	1.25	1.23	1.06	1.35	1.32	1.03
Pb	25.7	20.8	26.4	24.5	28.1	34.1	34.0	35.1	52.1	33.0	27.7	30.7
Th	15.9	14.5	15.8	14.7	16.5	17.3	16.4	15.7	7.3	17.4	21.3	17.3
U	4.20	3.68	3.33	2.30	5.79	7.74	3.70	4.13	3.84	12.0	10.3	4.31
LREEs/HREEs	4.96	4.78	4.67	5.26	5.26	6.05	4.40	5.29	1.74	4.33	5.15	4.83
Eu/Eu*	0.77	0.75	0.83	0.77	0.76	0.60	0.75	0.73	0.41	0.78	0.51	0.86
(La/Yb)N	16.07	15.85	13.46	17.27	18.84	23.55	15.57	18.47	5.281	13.72	17.98	16.25
Sr/Y	23.58	21.61	25.06	24.23	24.39	20.55	20.70	22.42	4.12	18.66	13.88	23.48
Nb/Ta	16.17	16.12	14.64	13.04	16.43	16.08	12.80	11.76	10.46	14.88	16.67	17.31
Wuchaba pluton												
Sample	XJB12–01	MDG12–01	MXB12–02	MXB12–03	DPC12–01	DBL12–01	MZG12–02	CJM12–01 (host)	CJM12–01 (MME)	CJM12–03	MK12–02	MK12–04
Major elements (wt.%)												
SiO_2	72.25	71.28	71.74	73.61	70.64	70.56	64.61	72.08	53.31	73.91	68.35	53.92
TiO_2	0.31	0.36	0.29	0.18	0.29	0.39	0.51	0.38	1.06	0.05	0.46	1.02
Al_2O_3	14.40	14.31	14.65	14.38	15.24	14.67	16.79	13.77	16.70	13.86	14.88	16.28
TFe_2O_3	2.09	2.30	1.75	1.52	2.11	2.60	3.51	2.54	9.52	0.48	3.39	7.89
MnO	0.06	0.06	0.03	0.02	0.04	0.05	0.08	0.06	0.28	0.03	0.07	0.17
MgO	0.60	0.73	0.48	0.31	0.54	0.87	1.05	0.83	3.48	0.12	1.08	3.73
CaO	1.55	1.84	0.97	0.96	1.34	1.85	1.67	3.07	4.69	0.90	2.62	4.81
Na_2O	3.52	3.42	3.47	3.48	3.69	3.46	3.19	3.98	3.43	4.00	3.43	3.17
K_2O	4.55	4.18	4.92	4.50	4.43	3.84	7.27	1.88	5.82	4.97	3.99	6.09
P_2O_5	0.12	0.15	0.12	0.13	0.11	0.16	0.20	0.18	0.39	0.04	0.13	0.56
LOI	0.45	0.74	0.81	1.42	0.66	0.73	0.78	0.42	0.51	0.72	0.76	0.76
$Na_2O + K_2O$	8.07	7.59	8.39	7.99	8.12	7.30	10.47	5.86	9.25	8.97	7.43	9.26
K_2O/Na_2O	1.29	1.22	1.42	1.29	1.20	1.11	2.28	0.47	1.70	1.24	1.16	1.92
A/CNK	1.02	1.03	1.06	1.09	1.09	1.10	0.93	1.09	0.82	0.95	1.02	0.97
Total	99.91	99.37	99.24	100.52	99.10	99.17	99.68	99.18	99.18	99.07	99.16	98.39
Trace elements (ppm)												
Li	123	117	140	62.9	131	77.5	106	47.1	134	46.4	120	168
P	444	467	464	288	492	544	752	523	1753	100	687	2381
K	40,940	45,080	47,500	46,920	44,060	37,700	68,560	16,512	65,860	46,060	41,440	57,344
Sc	4.55	4.97	2.91	2.42	3.66	4.59	6.67	6.88	23.3	2.25	6.62	17.1
Ti	2126	2584	1909	1229	2006	2662	3608	2428	7912	325.2	3338	6897
V	21.5	27.1	15.9	9.25	16.1	29.6	42.3	30.3	154	1.91	40.9	161
Cr	9.88	11.5	4.86	4.60	21.3	13.7	14.8	11.9	77.1	2.58	14.8	17.5
Mn	455	484	243	178	337	396	638	439	2422	202	583	1377
Co	3.10	3.86	2.13	1.33	2.70	4.35	5.59	3.75	17.1	0.08	5.21	18.4
Ni	3.56	4.73	3.55	2.13	13.1	6.46	5.96	3.56	16.0	1.29	5.33	8.40
Cu	1.47	2.62	1.63	1.76	2.86	4.08	2.22	2.94	66.1	0.585	3.29	3.56
Zn	61.5	54.8	78.7	106	58.0	63.0	98.5	58.0	160	22.9	76.1	101

Table 2 (continued)

Ga	21.4	23.1	25.4	25.6	25.9	21.9	23.6	19.9	25.5	19.6	23.3	18.8
Rb	271	257	310	295	283	215	341	113	368	339	261	328
Sr	234	313	184	146	215	303	364	315	226	32.6	329	428
Y	22.3	16.9	9.48	9.46	15.0	16.1	22.4	19.6	50.0	17.9	26.8	27.7
Zr	144	155	166	121	160	195	256	197	220	43.6	227	216
Nb	21.5	21.0	20.3	21.8	23.0	19.9	25.9	17.4	31.6	17.6	26.2	15.3
Cs	21.9	23.6	26.5	13.5	20.8	13.0	13.9	9.55	24.9	44.3	22.8	13.3
Ba	534	782	628	491	620	729	1222	245	541	38.3	661	846
La	30.6	31.8	34.6	28.6	35.6	26.2	63.8	38.1	34.8	8.96	36.9	36.3
Ce	59.2	59.4	70.0	55.9	68.6	59.4	119	73.1	69.6	19.1	71.1	75.6
Pr	6.51	6.38	7.20	5.95	7.29	5.50	12.89	7.88	8.61	2.13	7.93	9.18
Nd	23.8	22.6	25.3	20.8	25.9	19.9	45.5	28.9	36.6	7.74	29.5	36.4
Sm	4.95	4.47	4.68	3.98	4.90	4.15	7.87	5.70	10.47	2.38	6.25	7.69
Eu	0.82	0.93	0.79	0.65	0.83	0.83	1.34	0.95	0.93	0.14	1.08	1.60
Gd	4.40	3.94	3.45	3.04	3.96	3.66	6.14	4.99	10.9	2.69	5.65	7.14
Tb	0.64	0.56	0.40	0.37	0.53	0.51	0.76	0.67	1.65	0.49	0.80	0.96
Dy	3.67	3.09	1.91	1.83	2.71	2.86	3.94	3.58	9.53	2.95	4.52	5.06
Ho	0.70	0.57	0.32	0.31	0.49	0.53	0.73	0.66	1.78	0.56	0.87	0.93
Er	2.12	1.60	0.85	0.84	1.37	1.51	2.11	1.87	5.01	1.62	2.55	2.48
Tm	0.32	0.22	0.11	0.11	0.20	0.21	0.29	0.25	0.67	0.24	0.37	0.33
Yb	2.18	1.43	0.72	0.72	1.25	1.37	1.87	1.61	4.30	1.56	2.45	2.16
Lu	0.32	0.21	0.10	0.10	0.19	0.20	0.28	0.24	0.62	0.22	0.36	0.32
Hf	3.95	3.94	4.18	3.28	4.11	4.58	6.11	4.74	5.17	1.63	5.56	4.84
Ta	2.04	1.55	1.30	1.65	1.78	1.34	1.61	1.04	1.80	1.70	1.85	0.88
Pb	34.8	34.6	31.2	39.3	35.0	29.5	40.7	18.9	41.5	59.2	32.5	29.5
Th	18.4	14.7	18.7	15.6	19.8	14.9	29.8	17.1	9.2	6.5	18.5	8.88
U	3.76	4.23	4.14	4.86	2.93	3.75	5.48	6.43	6.50	4.58	6.50	2.45
LREEs/HREEs	3.43	4.40	8.22	6.91	5.57	4.30	6.49	4.63	1.90	1.44	3.45	3.55
Eu/Eu*	0.52	0.66	0.58	0.55	0.56	0.63	0.57	0.53	0.26	0.16	0.54	0.65
$(La/Yb)_N$	10.07	15.97	34.61	28.64	20.48	13.73	24.48	16.96	5.80	4.13	10.80	12.03
Sr/Y	10.47	18.52	19.41	15.41	14.34	18.80	16.21	16.13	4.52	1.82	12.29	15.47
Nb/Ta	10.56	13.59	15.66	13.22	12.92	14.87	16.06	16.70	17.52	10.34	14.18	17.38
Eu/Eu*	0.52	0.66	0.58	0.55	0.56	0.63	0.57	0.53	0.26	0.16	0.54	0.65
$(La/Yb)_N$	10.07	15.97	34.61	28.64	20.48	13.73	24.48	16.96	5.80	4.13	10.80	12.03
Sr/Y	10.47	18.52	19.41	15.41	14.34	18.80	16.21	16.13	4.52	1.82	12.29	15.47
Nb/Ta	10.56	13.59	15.66	13.22	12.92	14.87	16.06	16.70	17.52	10.34	14.18	17.38

$(La/Yb)_N$ is normalizedby Chondrite,Chondrite values are from Sun and McDonough (1989)

A/CNK molar $Al_2O_3/(CaO + Na_2O + K_2O)$, *A/NK* molar $Al_2O_3/(Na_2O + K_2O)$, *Eu/Eu** $W(Eu)_N/[(1/2)(W(Sm)_N + W(Gd)_N)]$

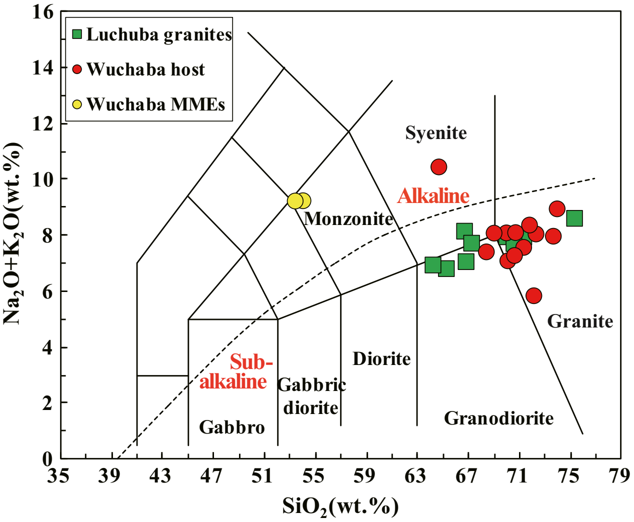

Fig. 6 Total alkalis ($Na_2O + K_2O$) versus SiO_2 (TAS) diagram showing the compositional variation of Luchuba and Wuchaba samples. The MMEs are less felsic than the hosts

isotopic characteristics of $I_{Sr}(t)$ = 0.7069 to 0.7080, $\varepsilon_{Nd}(t)$ = −9.86 to −3.34 and $\varepsilon_{Hf}(t)$ = −5.69 to 1.58. The two MMEs of Wuchaba granitoids also show Sr-Nd-Hf isotopic compositions ($I_{Sr}(t)$ is 0.7069 and 0.7073, $\varepsilon_{Nd}(t)$ = −4.74 and −3.34, $\varepsilon_{Hf}(t)$ = −0.78 and 1.58) comparable to those of Wuchaba host. Sample ZKL12–01 of the Luchuba pluton gives very high $^{87}Sr/^{86}Sr$ of 0.737981. This high ratio is consistent with the high Rb/Sr ratio resulting from significant extent of plagioclase-dominated fractional crystallization (also low in Ba, P, and Ti; see Fig. 9). The high $^{87}Rb/^{86}Sr$ ratio (10.50) makes the calculated $I_{Sr}(t)$ unreliable (Jahn et al. 2000).

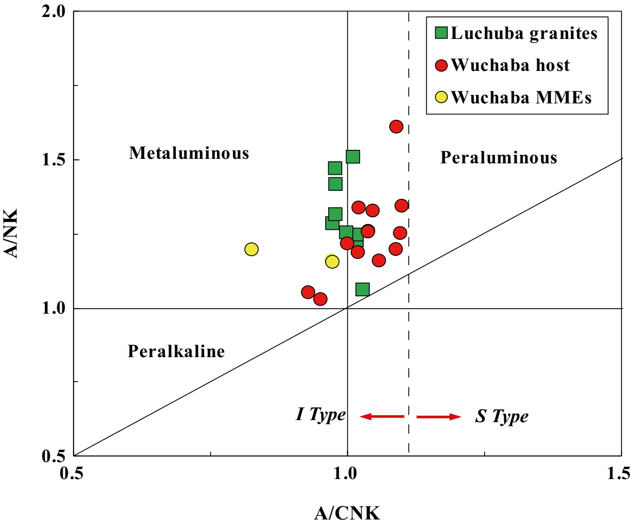

Fig. 7 Diagram of A/NK [$Al_2O_3/(Na_2O + K_2O)$] vs. A/CNK [molar ratio $Al_2O_3/(CaO + Na_2O + K_2O)$] for granitoids of Luchuba and Wuchaba plutons in WQOB

Discussion

Assimilation and fractional crystallization (AFC)

The data shown in SiO_2-variation diagrams (Fig. 8) are to a first-order consistent with varying extent of fractional crystallization of hornblende, plagioclase, Fe–Ti oxides and apatite. However, these trends are also consistent with modal variations of these phases in the samples although the depletion in P, Nb, Ta and Ti emphasizes the significance of fractional crystallization. These granitoids display sub-chondritic Nb/Ta ratio, which is also consistent with hornblende controlled fractionation ($Kd_{\text{hornblende}}$ Nb/Ta = 1.40) (Foley et al. 2002). The moderately to strongly negative anomalies of Ba, Sr and Eu (Figs. 9 and 10) indicate extensive fractionation of plagioclase and/or K-feldspar (Wu et al. 2003). The scattered data in the I_{Sr} vs. 1/Sr and $\varepsilon_{Nd}(t)$ vs. 1/Nd plots (Fig. 11) suggest that the petrogenesis of samples from the two plutons was controlled by fractional crystallization and contamination (Xing and Xu, 1996). While scattered, it is apparent in Fig. 12 that the two plutons show quite similar range of initial $^{87}Sr/^{86}Sr$ values (except for sample ZKL12–01 with high Rb/Sr) while the $\varepsilon_{Nd}(t)$ and $\varepsilon_{Hf}(t)$ values decrease with increasing SiO_2, which is consistent with fractional crystallization, accompanied by increased crustal contamination/assimilation. It is should be noted that the small variation of Sr isotopes reflects similar Sr isotope composition of the actually contaminated crust. All these data signify that assimilation–fractional crystallization (AFC) processes (DePaolo 1981) played a role in the petrogenesis of the two plutons.

Petrogenesis of granitoids

Generally, granitoids are typically divided into I-, S-, A- and M-type in terms of source rock types and petrogenesis (e.g., Chappell and White 1974; Collins et al. 1982; Whalen 1985). Amphibole, cordierite, and alkaline minerals are important diagnostic minerals for discriminating I-, S- and A-type granites respectively. The absence of aluminous minerals such as muscovite, tourmaline and garnet, combined with the magmatic assemblage of hornblende and biotite (Fig. 3), and the relatively low A/CNK values (<= 1.1, Fig. 7) is consistent with these granitoids being of I-type.

The Luchuba and Wuchaba plutons have low $(La/Yb)_N$ and Sr/Y, suggesting that their parental magmas were generated under relatively low pressures (~ 40 km) without garnet being present as the residual phase in the magma source region or as liquidus phase during magma evolution (e.g., Martin et al. 2005; Klein et al. 2000; Pertermann et al. 2004). Here we emphasize a maximum depth of ~40 km for melt formation because of the lack of garnet signature in the two granitoid plutons (Mo et al. 2008).

Table 3 Sr, Nd, Hf isotopes of the Luchuba and Wuchaba pluton

Sample	$^{87}Rb/^{86}Sr$	$^{87}Sr/^{86}Sr$	2σSE	$I_{Sr}(t)$	$^{147}Sm/^{144}Nd$	$^{143}Nd/^{144}Nd$	2σSE	$\varepsilon_{Nd}(t)$	$^{176}Lu/^{177}Hf$	$^{176}Hf/^{177}Hf$	2σSE	$\varepsilon_{Hf}(t)$
SEB12–01	1.18	0.711734	0.000006	0.7080	0.113	0.512173	0.000003	-6.72	0.006652	0.282595	0.000005	-2.40
BSB12–01	1.33	0.712454	0.000005	0.7083	0.124	0.512228	0.000004	-5.95	0.008734	0.282623	0.000006	-1.71
YDB12–03	1.24	0.712255	0.000005	0.7084	0.110	0.512170	0.000004	-6.69	0.007063	0.282587	0.000005	-2.74
YDB12–05	1.44	0.712253	0.000006	0.7077	0.112	0.512223	0.000003	-5.73	0.007126	0.282618	0.000003	-1.65
LTB12–01	2.16	0.717152	0.000006	0.7104	0.116	0.512150	0.000004	-7.25	0.007290	0.282567	0.000006	-3.48
ZKL12–01	10.50	0.737981	0.000016	0.7051	0.161	0.512171	0.000003	-8.11	0.018453	0.282522	0.000005	-6.70
DBQ12–01	2.14	0.713920	0.000006	0.7072	0.120	0.512218	0.000009	-6.05	0.007603	0.282613	0.000007	-1.90
MXB12–02	4.85	0.723182	0.000006	0.7080	0.112	0.512171	0.000009	-6.74	0.003485	0.282592	0.000005	-2.04
DPC12–01	3.81	0.719421	0.000006	0.7075	0.115	0.512163	0.000009	-6.98	0.006547	0.282606	0.000003	-1.99
MZG12–02	2.71	0.715710	0.000017	0.7072	0.105	0.512220	0.000011	-5.59	0.006554	0.282602	0.000005	-2.13
CJM12–01(host)	1.04	0.711114	0.000008	0.7079	0.120	0.512245	0.000010	-5.52	0.007084	0.282614	0.000006	-1.79
CJM12–01(MME)	4.70	0.721585	0.000005	0.7069	0.174	0.512363	0.000008	-4.74	0.016965	0.282683	0.000006	-0.78
CJM12–03	30.07	0.785554	—	—	0.187	0.512119	0.000012	-9.86	0.019316	0.282554	0.000006	-5.69
MK12–02	2.28	0.714738	0.000005	0.7076	0.129	0.512285	0.000008	-4.98	0.009231	0.282625	0.000005	-1.71
MK12–04	2.22	0.714264	0.000006	0.7073	0.129	0.512369	0.000007	-3.34	0.009248	0.282718	0.000006	1.58

Where,*t* crystallization time of zircon (~220 Ma).$^{87}Rb/^{86}Sr$,$^{147}Sm/^{144}Nd$,$^{176}Lu/^{177}Hf$ ratios calculated using Rb, Sr, Sm and Nd contents, measured by ICP-MS.

$(^{147}Sm/^{144}Nd)_{CHUR} = 0.1967$, $(^{143}Nd/^{144}Nd)_{CHUR} = 0.512638$;$(^{176}Lu/^{177}Hf)_{CHUR} = 0.0332$, $(^{176}Hf/^{177}Hf)_{CHUR} = 0.282772$ (Blichert-Toft and Albarède, 1997)

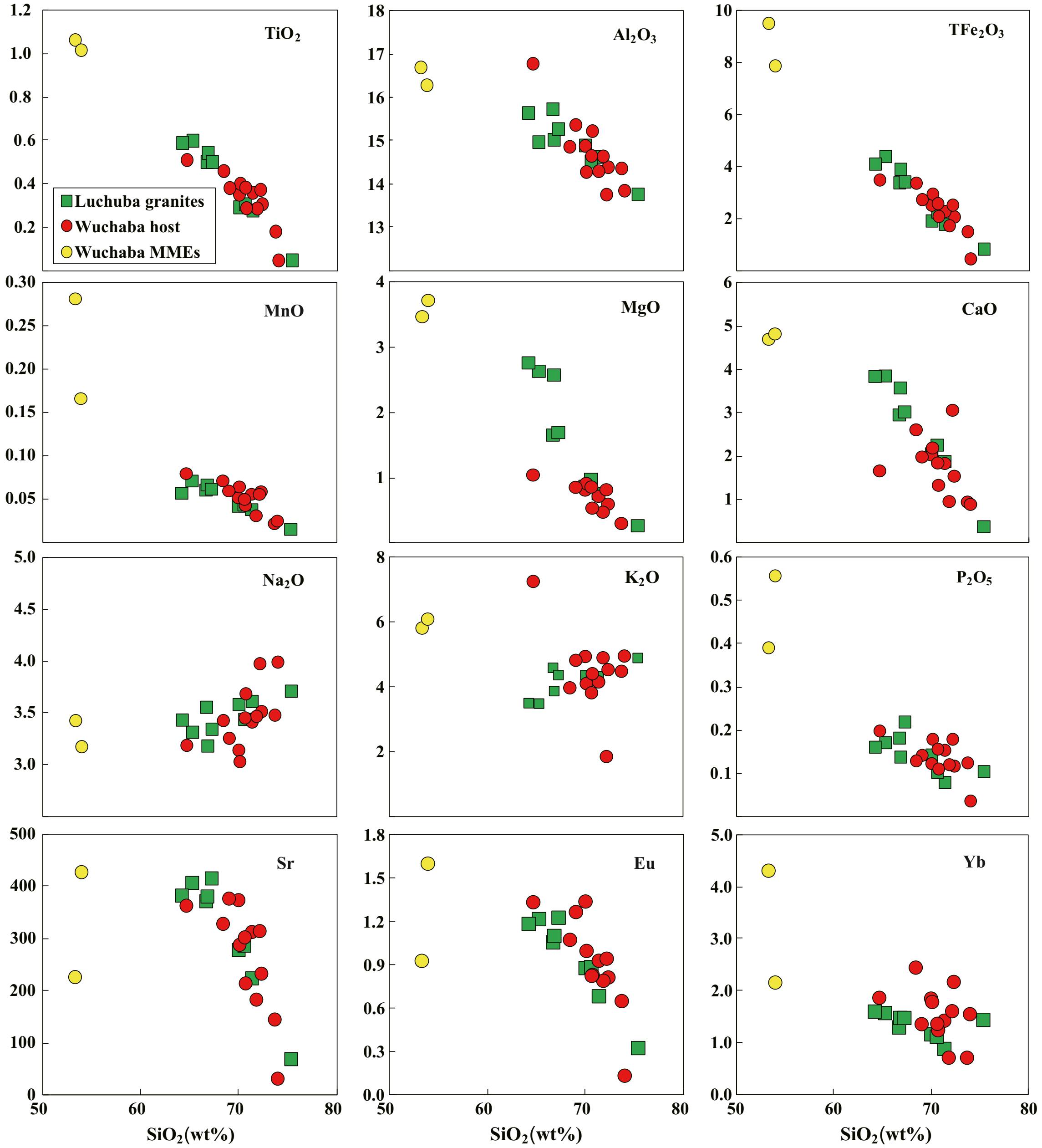

Fig. 8 SiO_2 variation diagrams of representative major elements (wt.%) and selected trace elements (ppm) of Luchuba and Wuchaba samples

Partial melting of the lower continental crust may account for the origin of granitic rocks, and some authors argued that the magma sources for the WQOB granitoids could be basic rocks (amphibolite) (Zhang et al. 2007). However, the dehydration melting of amphibolite in the lower crust should result in melts high in Na_2O and low in K_2O (Beard and Lofgren 1991), which is inconsistent with the high-K characteristics of the Luchuba and Wuchaba plutons. Besides, partial melting of the basaltic source usually needs higher melting temperature and amphibole dehydration melting cannot produce such volumetrically significant granitoids. Thus, the origin by partial melting of pre-existing mafic lower crust is less likely. The Luchuba and Wuchaba plutons, as other coeval granites elsewhere in the WQOB, have lower $(^{87}Sr/^{86}Sr)_i$, higher $\varepsilon_{Nd}(t)$ and $\varepsilon_{Hf}(t)$ than the mature continental crust ($[^{87}Sr/^{86}Sr]_i > 0.72$, $\varepsilon_{Nd}(t) < -12$) (Fig. 13a) (Zhang et al. 2007). Hence, it is unlikely that these granitoids were produced by melting of mature continental crust (upper crust) ($[^{87}Sr/^{86}Sr]_i > 0.72$, $\varepsilon_{Nd}(t) < -12$) (Niu and O'Hara, 2009), but has significant mantle contribution (or juvenile crustal material) in terms of isotopes. In addition, Hf-Nd isotopes are coupled and lie in the global mantle and crustal array (Fig. 13b) indicating mantle (or juvenile continental crust) contribution. In the age-$\varepsilon_{Hf}(t)$ diagram (Fig. 13c), the majority of samples fall between

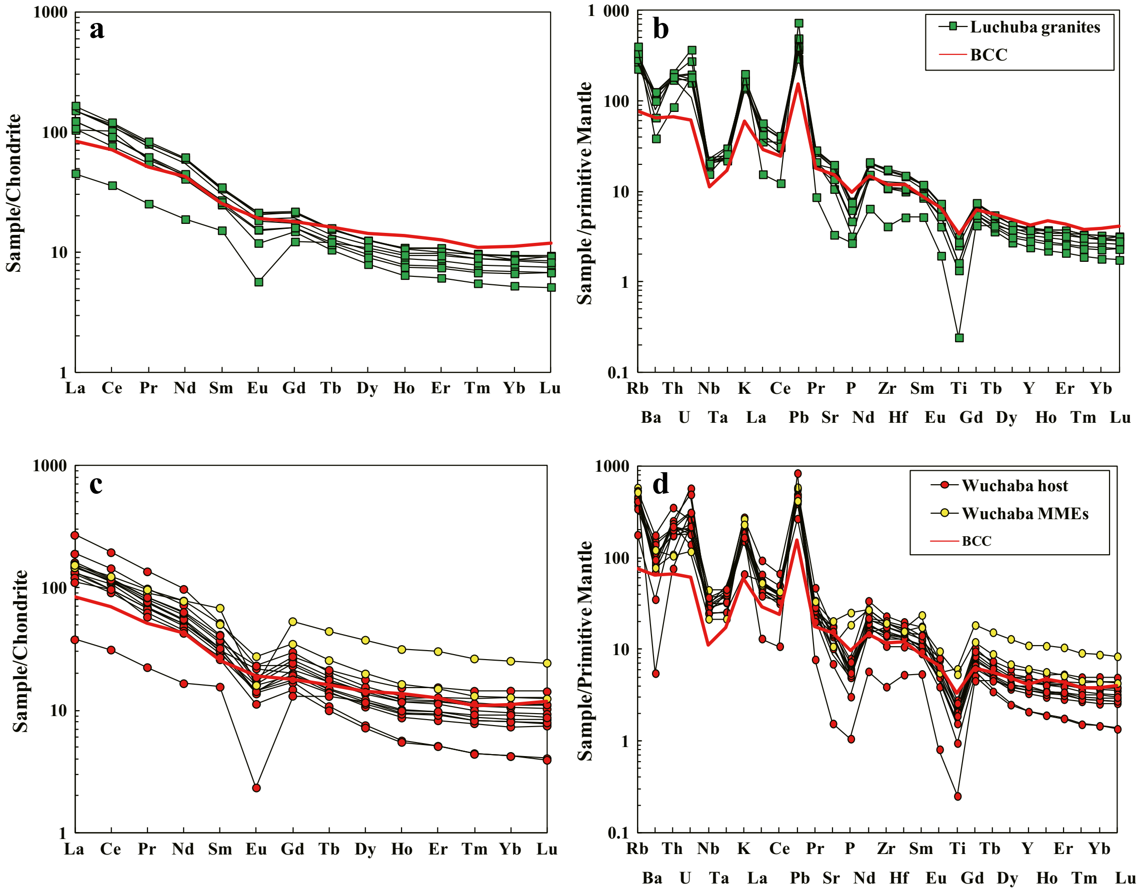

Fig. 9 **(a)** Chondrite normalized REE patterns, and **(b)** Primitive mantle normalized incompatible element patterns of samples from Luchuba pluton; **(c)** Chondrite normalized REE patterns, and **(d)** Primitive mantle normalized incompatible element patterns of samples from Wuchaba pluton. For comparison, the average bulk continental crust (BCC, red solid line) (Rudnick and Gao 2003) is also plotted. Chondrite and primitive mantle values are from Sun and McDonough (1989)

the mantle and crustal evolution line, also indicating significant mantle contribution for these granitoids (Wang et al. 2012). Additionally, pioneering studies (Dong et al. 2011, 2012) suggest that the Paleo-Tethys Mianlue Ocean was already closed at the time of granitoids emplacement (~ 220 Ma). Therefore, we suggest that the Luchuba and Wuchaba plutonism was a response to continental collision. In the context of continental collision, reasonable mechanism for granitoid magmatism with significant mantle isotopic signature was discussed by Niu et al. (2013). Partial melting of subducted basaltic ocean crust (Mianlue MORB) under amphibolite facies conditions can produce andesitic melts resembling bulk continental crust (BCC) (Niu et al. 2013; also see below). Note that the lack of adakite signature (i.e., high Sr/Y and La/Yb; Defant and Drummond 1990; Castillo 2006 2012) requires melting under amphibolite facies conditions (see Niu et al. 2013). In this study, the Luchuba and Wuchaba plutons have REE and trace element patterns resembling those of the BCC (Fig. 9). Despite the felsic compositions with radiogenic Sr and unradiogenic Nd of the Luchuba and Wucbaba plutons, they have higher $\varepsilon_{\mathrm{Nd}}(t)$ value than typical continental crust, especially their high $\varepsilon_{\mathrm{Hf}}(t)$ values are close to zero (see above). Simple isotopic

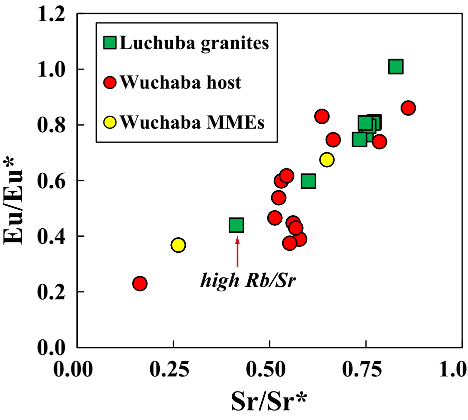

Fig. 10 Plot of Sr/Sr* vs. Eu/Eu* for the Luchuba and Wuchaba granitoids. $\mathrm{Sr/Sr^*} = \mathrm{Sr_{PM}}/[1/2^*(\mathrm{Pr_{PM}} \times \mathrm{Nd_{PM}})]$; $\mathrm{Eu/Eu^*} = \mathrm{Eu_{PM}}/[1/2^*(\mathrm{Sm_{PM}} \times \mathrm{Gd_{PM}})]$; Primitive mantle values are from Sun and McDonough (1989)

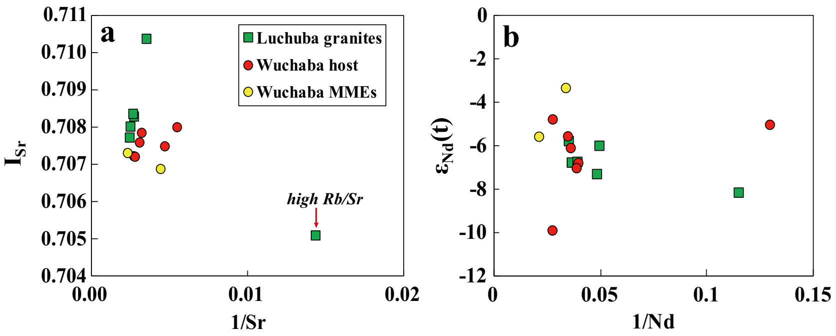

Fig. 11 **(a)** Plot of I_{Sr} vs. 1/Sr for the Luchuba and Wuchaba granitoids. **(b)** Plot of $\varepsilon_{Nd}(t)$ vs. 1/Nd for the Luchuba and Wuchaba granitoids

mixing calculations suggest that ~50% ocean crust (MORB) contributes to the source of the Luchuba and Wuchaba plutons (Fig. 14). Hence, the syncollisional plutons represent juvenile crust with primary materials isotopically coming from the mantle. In this case, the remaining part of the Mianlue oceanic crust is most likely the best source for generating andesitic magmas parental to the Luchuba and Wuchaba plutons; partial melting of the basaltic oceanic crust produces felsic melts and the ocean crust derived from the mantle not long ago imparts the mantle isotopic signature (Niu et al. 2013). Meanwhile, AFC during magma ascent can explain the crustal signatures of the Luchuba and Wuchaba granitoids.

Origin of MMEs

Both Luchuba and Wuchaba plutons contain mafic magmatic enclaves (MMEs). The origin of the MMEs is key to the petrogenesis of the granitoids. Three models have been proposed to explain the origin of MMEs: (1) restites (Chen et al. 1989; Chappell et al. 2000); (2) representing mantle derived melts (Barbarin 2005; Mo et al. 2007; Yang et al. 2007; Clemens and Stevens 2011); (3) mafic cumulate of the same magmatic system with the host (Wall et al. 1987; Dahlquist 2002; Niu et al. 2013; Huang et al. 2014; Chen et al. 2015, 2016). The MMEs in the Wuchaba pluton (1) have the same magmatic

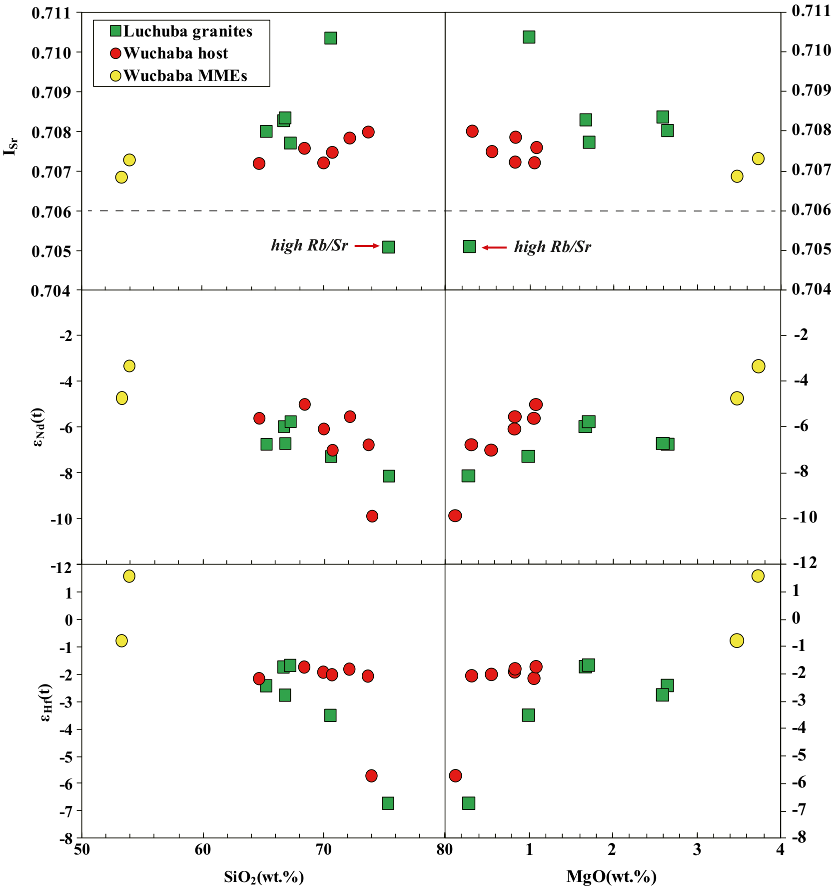

Fig. 12 Plots of Sr, Nd and Hf isotopes (in the forms of initial $^{87}Sr/^{86}Sr$ or I_{Sr}, $\varepsilon_{Nd}(t)$ and $\varepsilon_{Hf}(t)$) against MgO and SiO_2

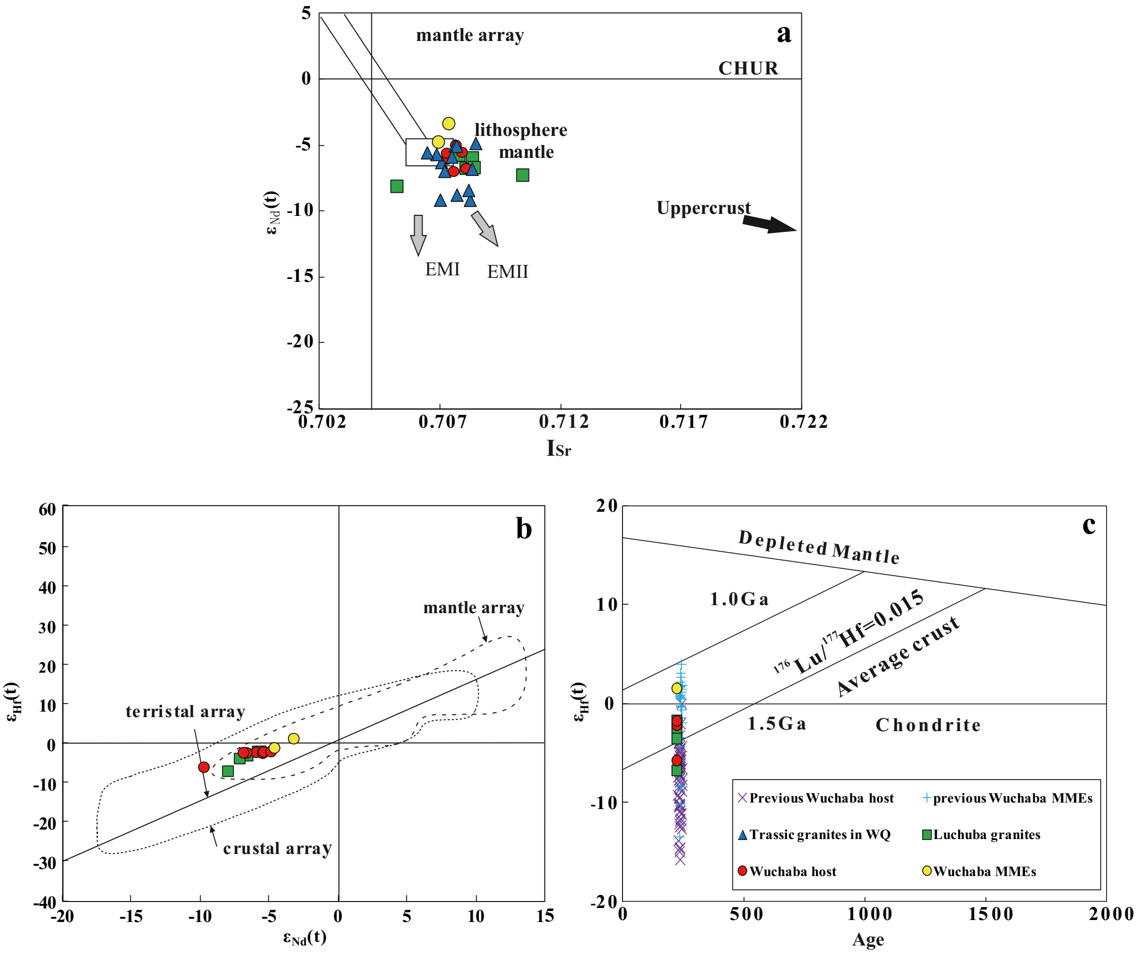

Fig. 13 **(a)** $\varepsilon_{Nd}(t)$ vs. I_{Sr} plot of the Luchuba and Wuchaba granitoids (modified after Qin et al. 2009); the data for the Triassic granites in western Qinling are from Zhang et al. (2007). **(b)** $\varepsilon_{Nd}(t)$ vs. $\varepsilon_{Hf}(t)$ plot. The field for crust-mantle array is from Vervoort et al. (1999) and the terrestrial array is from Vervoort et al. (2011). **(c)** Age (Ma) vs. $\varepsilon_{Hf}(t)$ plot of the Luchuba and Wuchaba granitoids, together with the literature Hf isotope data (Zhu et al. 2013)

mineralogy as the host and a fine-grained texture without any disequilibrium features such as crystal resorption or reactive overgrowth (Fig. 3d), which, together with lacking metamorphic or residual sedimentary fabrics, rules out the restite origin; (2) the similar U-Pb ages of both MMEs and the host (e.g., Zhu et al. 2013) also argue against the restite model; (3) the MMEs have greater amphibole modes with cumulate texture formed by hornblende-plagioclase; (4) MMEs have slightly higher $\varepsilon_{Nd}(t)$ or $\varepsilon_{Hf}(t)$ than their host granitoids and have similar Sr isotopes (Fig. 12). The similar isotope variation ranges for both granitoid hosts and the MMEs are inconsistent with mafic-felsic magma mixing, but are consistent with the same mantle source with varying extents of crustal contamination as discussed above (Figs. 11 and 12).

Many authors still follow the popular view that the similar Sr-Nd-Hf isotope between the host and MMEs have resulted from magma mixing. We emphasize that it is physically unlikely that isotopes become homogenized whereas major and trace elements are not (Niu et al. 2013; Chen et al. 2015). It also should be noted that the MMEs and host rocks have significant linear trends in SiO_2 variation diagrams (Fig. 8), which could be interpreted as magma mixing, but they are more consistent with fractional crystallization with superimposed/enhanced effects of modal mineralogy. It is important to note that the fine grain size of MMEs is no evidence against their cumulate origin, but evidences a cumulate origin at an early stage of magma cooling when magma was emplaced in a new and relatively cold ambient crust; the first major liquidus phases are amphibole (± biotite ± plagioclase) and rapid quenching will facilitate abundant nucleation without between-nuclei space for growth, thus forming fine-grained MME cumulates (Chen et al. 2015). Therefore, we maintain that the MMEs represent disturbed earlier cumulate of the same magmatic system.

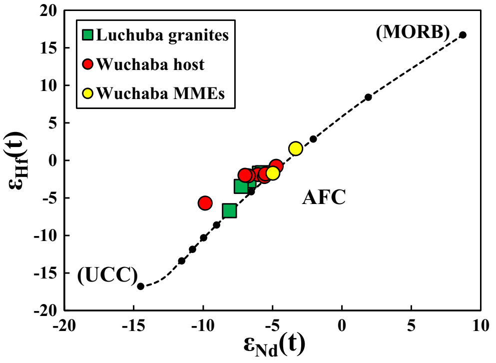

Fig. 14 Plot of $\varepsilon_{Nd}(t)$ vs. $\varepsilon_{Hf}(t)$ for Luchuba and Wuchaba granitoids. The modeled AFC path uses parental magma (Mianlue MORB) with 6.5 ppm Nd ($\varepsilon_{Nd}(t)$: 8.71) and 1.87 ppm Hf ($\varepsilon_{Hf}(t)$: 16.7) (Xu et al. 2002) and a mature continental crust with 26 ppm Nd ($\varepsilon_{Nd}(t)$: −14.5) and 5.8 ppm Hf ($\varepsilon_{Hf}(t)$: −16.8) (Shen et al. 1997) for conceptual simplicity. The Hf isotope composition for MORB is inferred from Nd isotope according to the equation ($\varepsilon_{Hf} = 1.59\varepsilon_{Nd} + 1.28$) given by (Chauvel et al. 2008), for continental crust according to the equation ($\varepsilon_{Hf} = 1.36\varepsilon_{Nd} + 2.95$) given by (Vervoort et al. 1999). AFC path calculated according to (Depaolo, 1981) equation. The ratio of assimilation to fractionation was set at $r = 0.5$. Bulk Kd's for Nd and Hf were 0.4 and 0.6, respectively. The partition coefficients of Nd and Hf for amphibole and plagioclase are from Bacon and Druitt (1988) and for biotite from Schnetzler and Philpotts (1970) and Higuchi and Nagasawa (1969)

Geodynamic implications

The Qinling orogenic belt culminated with the collision of the Yangtze Block (YB) with the North China Craton (NCC) in the Mid-Late Triassic along the Mianlue suture zone (Chen et al. 2000, 2010; Liu et al. 2005; Jiang et al. 2010; Li et al. 2011; Dong et al. 2011, 2012, 2013, 2016; Ni et al. 2012). The age data show that the NCC-YB collision occurred between 234 and 220 Ma (Sun et al. 2002a; Zhu et al. 2009; Qin et al. 2010; Liu et al., 2011a, b; Dong et al. 2012; Li et al. 2013, 2015). The Luchuba and Wuchaba granitoids have identical crystallization ages to other late Triassic granitoids in the WQOB (Zhang et al. 2007). The popular explanation is that slab break off along the Qinling-Dabie orogen occurred at shallow depth causing asthenosphere upwelling and lower crust melting causing widespread Triassic granitoid magmatism (Sun et al. 2002a). However, it is physically difficult to have asthenosphere upwelling without significant mantle lithosphere delamination (removal) and lower crust melting. In fact, continuous lithosphere extension and delamination in the WQOB occurred at <210 Ma (Yang et al. 2012). Other authors postulated a thermal pulse associated with the slab break off resulting from the asthenosphere upwelling along the Mianlue suture during the Late Triassic; the upwelling triggered partial melting of the Neoproterozoic SCLM that generated the MME and the partial melting of the Neo-Mesoproterozoic lower crust for the granitic magmatism (Qin et al. 2009; Zhu et al. 2013). The MMEs are of cumulate origin with the hornblende-plagioclase assemblage of the same magmatic system as the host granitoid rather than representing mafic magmas of SCLM origin (see Huang et al. 2014; Chen et al. 2015, 2016). Hence, partial melting of Mesoproterozoic crustal rocks and melt interaction with sub-continental lithospheric mantle (SCLM) is also implausible.

The magma emplacement ages for the Luchuba and Wuchaba granitoids broadly coincide with the timing of the NCC-YB collision. It is remarkable that the Nb-Ta-Ti depletion and the subchondritic Nb/Ta ratio are characteristic of these granitoids without invoking active subduction-zone magmatism; subduction-related magmatism would produce variably high excess Sr that is inconsistent with the Sr deficiency of the granitoids (Fig. 9). Therefore, we suggest that in the late Triassic the WQOB witnessed a period of syn-collisional granitoid magmatism not subduction-related magmatism. The following scenario is proposed to explain the petrogenesis of the Luchuba and Wuchaba granitoids.

We argue that the YB-NCC collision began at ~220 Ma (Fig. 15) and finished ~210 Ma (see discussion above). Upon collision, the Mianlue oceanic crust (as old as ~350 Ma; Xu et al. 2002) that had been subducted beneath the Qinling active (Andean-type) continental margin (Dong et al. 2012) may have undergone melting producing the melts parental to the Luchuba and Wuchaba granitoids. It is possible and likely that the Mianlue oceanic crust reached temperatures in excess of 800 °C with continued underthrusting to produce significant amounts of melt. Because during Triassic subduction to collision hot thermal conditions prevailed at an active continental margin with a geotherm >20 °C/km well within the melting conditions (Kelemen et al. 2003). Therefore, the remaining Mianlue oceanic crust was continuously and slowly

Fig. 15 Proposed tectonic model for the generation of the Luchuba and Wuchaba granitoids in West Qinling during the late Triassic (~220 Ma). See text for explanation

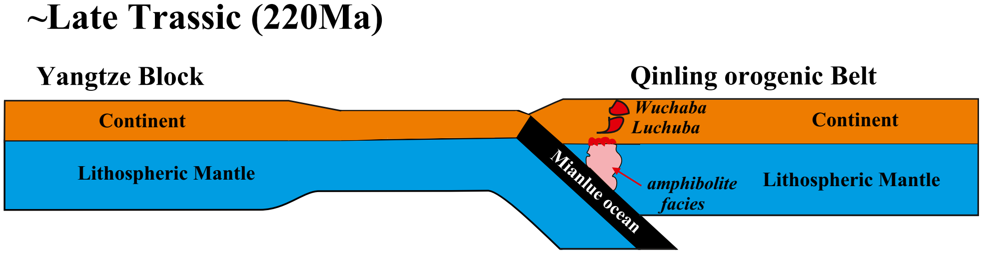

subducted along high T/P paths (as attaining thermal equilibrium with the superjacent hot active continental margin) resulting in enhanced heating at the early stage of YB-NCC collision.The underthrusting Mianlue ocean crust began to melt when passing through the hydrous basaltic/granitic solidus (<650 °C) under amphibolite facies conditions (Mo et al. 2008, Niu et al. 2013). Such conditions and processes can produce andesitic melts parental to the Luchuba and Wuchaba granitoids. It is noteworthy that we emphasized melting of MORB under amphibolite facies conditions not amphibole dehydration melting which requires much higher temperature (>850 °C, Rushmer 1991). The latter can hardly produce volumetrically significant granitoids (see above). These granitoids resemble the composition of the BCC without the Y or HREE depleted "garnet signature", in support of melting under amphibolite facies conditions without garnet present as a residual phase (details see Sr–Nd–Hf isotopes section in Niu et al. 2013). The andesitic parental magma when emplaced in a magma chamber would rapidly cool and crystallize mafic minerals (e.g., hornblende, biotite) and plagioclase to form fine-grained cumulates (MMEs), which can be readily disturbed by replenishing magmas, leading to the more mafic cumulate to becoming dispersed as MMEs in the granitoid host. Our model is consistent with open-system magma chamber processes with continued evolution (fractional crystallization)/replenishment accompanied by crustal contamination and assimilation.

Conclusions

1. Zircon U-Pb dating yields ages of 211 ± 1.4 Ma and 218.5 ± 2.3 Ma for the Luchuba pluton and of 218.7 ± 1.3 Ma for the Wuchaba pluton, respectively. This is within the age range of the collision of the Yangtze Block with the North China Craton.
2. The granitoids of the Luchuba and Wuchaba plutons display an enriched LILE and LREE patterns and have variable negative Eu anomalies, which is similar to, but more evolved than, those of bulk continental crust. Our results suggest that the Luchuba and Wuchaba plutons are best explained by melting of amphibolite of MORB protolith (the Paleo-Tethys Mianlue ocean crust) during continental collision, which produced granitic melts with a remarkable compositional similarity to the BCC with inherited mantle-like isotopic compositions modified by AFC process-like assimilation.
3. MMEs of Wuchaba pluton are earlier cumulates of the same magmatic system.
4. Ocean crust (MORB-like) contributes to the source of the Luchuba and Wuchaba granitoids, pointing to the significance of ocean crust melting in contributing to the continental crust accretion.

Acknowledgements We thank Cui Huixia, Gong Hongmei, Guo Pengyuan, Hu Zhenxing, Liu Jinju, Ma Yuxin, Sun Pu, Sun Wenli, Wang Xiaohong, Ye Lei, Ye Xiaolu and Zhang Guorui for assistance with sample preparation. We particularly thank Su Li for major and trace element analysis and zircon analysis and Ma Jinlong for Sr-Nd-Hf isotope analysis. This work was supported by grants from National Natural Science Foundation of China (41130314, 91014003), Chinese Academy of Sciences, regional and local authorities (Shandong Province and City of Qingdao) and Qingdao National laboratory of ocean sciences and Technology.

References

Andersen T (2002) Correction of common lead in U–Pb analyses that do not report ^{204}Pb. Chem Geol 192:59–79

Bacon CR, Druitt TH (1988) Compositional evolution of the zoned calcalkaline magma chamber of mount Mazama, crater Lake, Oregon. Contrib Mineral Petrol 98:224–256

Barbarin B (2005) Mafic magmatic enclaves and mafic rocks associated with some granitoids of the central sierra Nevada batholith, California: nature, origin, and relations with the hosts. Lithos 80: 155–177

Beard J, Lofgren G (1991) Partial melting of basaltic and andesitic greenstones and amphibolites under dehydration melting and water-saturated conditions at 1, 3, and 6.9 kilobars. J Petrol 32:365–401

Blichert-Toft J, Albarède F (1997) The Lu-Hf isotope geochemistry of chondrites and the evolution of the mantle-crust system. Earth Planet Sci Lett 148:243-258

Cao XF, Lü XB, Yao SZ, Mei W, Zou XY, Chen C, Liu ST, Zhang P, Su YY, Zhang B (2011) LA–ICP–MS U–Pb zircon geochronology, geochemistry and kinetics of the Wenquan ore-bearing granites from west Qinling, China. Ore Geol Rev 3:120–131

Castillo PR (2006) An overview of adakite petrogenesis. Chin Sci Bull 51:257–268

Castillo PR (2012) Adakite petrogenesis. Lithos 134:304–316

Chappell BW, White AJR (1974) Two contrasting granite types. Pacific Geol 8:173–174

Chappell BW, White AJR, Williams IS, Wyborn D, Wyborn LAI (2000) Lachlan Fold Belt granites revisited: high- and low-temperature granites and their implications. Aust J Earth Sci 47:123–138

Chauvel C, Lewin E, Carpentier M, Arndt NT, Marini JC (2008) Role of recycled oceanic basalt and sediment in generating the Hf–Nd mantle array. Nat Geosci 1:64–67

Chen YJ (2010) Indosinian tectonic setting, magmatism and metallogenesis in Qinling orogen, Central China. Geol China 37: 854–865 (in Chinese with English abstract)

Chen YJ, Li C, Zhang J, Li Z, Wang HH (2000) Sr and O isotopic characteristics of porphyries in the Qinling molybdenum deposit belt and their implication to genetic mechanism and type. Sci China Ser D 43(Suppl. 1):82–94

Chen S, Niu YL, Sun WL, Zhang Y, Li JY, Guo PY, Sun P (2015) On the origin of mafic magmatic enclaves (MMEs) in syn-collisional granitoids: evidence from the Baojishan pluton in the north Qilian orogen, China. Miner Petrol 109:1–20

Chen S, Niu YL, Li JY, Sun WL, Zhang Y, Hu Y, Shao FL (2016) Syn-collisional adakitic granodiorites formed by fractional crystallization: insights from their enclosed mafic magmatic enclaves (MMEs) in the Qumushan pluton, north Qilian orogen at the northern margin of the Tibetan plateau. Lithos 248:455–468

Clemens JD, Stevens G (2011) What controls chemical variation in granitic magmas. Lithos 134-135:317–329

Collins WJ, Beams SD, White AJR, Chappell BW (1982) Nature and origin of A-type granites with particular reference to southeastern Australia. Contrib Mineral Petrol 80:189–200

Corfu F, Hanchar JM, Hoskin PWO, Kinny P (2003) Altas of zircon textures. Rev Mineral Geochem 53:469–500

Chen YD, Price RC, White AJR (1989) Inclusions in Three S-Type Granites from Southeastern Australia. J Petrol 30:1181-1218

Dahlquist J (2002) Mafic microgranular enclaves: early segregation from metaluminous magma (sierra de Chepes), Pampean ranges, NW Argentina. J S Am Earth Sci 15:643–655

Defant MJ, Drummond MS (1990) Derivation of some modern arc magmas by melting of young subducted lithosphere. Nature 347: 662–665

Depaolo DJ (1981) Trace element and isotopic effects of combined wallrock assimilation and fractional crystallization. Earth Planet Sci Lett 53:189–202

Dong YP, Santosh M (2016) Tectonic architecture and multiple orogeny of the Qinling Orogenic Belt, Central China. Gondwana Res 29:1–40

Dong YP, Zhang GW, Neubauer F, Liu XM, Genser J, Hauzenberger C (2011) Tectonic evolution of the Qinling orogen, China: review and synthesis. J Asian Earth Sci 41:213–237

Dong YP, Liu XM, Zhang GW, Chen Q, Zhang XN, Li W, Yang C (2012) Triassic diorites and granitoids in the Foping area: constraints on the conversion from subduction to collision in the Qinling orogen, China. J Asian Earth Sci 47:123–142

Dong YP, Liu XM, Neubauer F, Zhang GW, Tao N, Zhang YG, Zhang XN, Li W (2013) Timing of Paleozoic amalgamation between the North China and South China blocks: evidence from detrital zircon U-Pb ages. Tectonophysics 586:173–191

Feng YM, Cao XZ, Zhang EP, Hu YX, Pan XP, Yang JL, Jia QZ, Li WM (2002) Structure, orogenic processes and geodynamic of the western Qinling orogen (in Chinese). Xi'an map press, Xi'an, pp:1–263

Foley SF, Barth MG, Jenner GA (2000) Rutile/melt partition coefficients for trace elements and an assessment of the influence of rutile on the trace element characteristics of subduction zone magmas. Geochim Cosmochim Acta 64:933–938

Foley S, Tiepolo M, Vannucci R (2002) Growth of early continental crust controlled by melting of amphibolite in subduction zones. Nature 417:837–840

Gao T (2011) The LA-ICP-MS zircon U-Pb dating, geology and geochemistry, tectonic setting of several important intrusions from the north part of the western stage of west Qinling and their relationship with mineralization. PhD thesis, Chang'an University, Xi'an

Hanchar JM, Hoskin PWO (2003) Zircon. Rev Mineral Geochem 53:1–500

Higuchi H, Nagasawa H (1969) Partition of trace elements between rock-forming minerals and the host volcanic rocks. Earth Planet Sci Lett 7:281–287

Huang H, Niu YL, Nowell G, Zhao ZD, Yu XH, Zhu DC, Mo XX, D S (2014) Geochemical constraints on the petrogenesis of granitoids in the east Kunlun orogenic belt, northern Tibetan plateau: implications for continental crust growth through syn-collisional felsic magmatism. Chem Geol 370:1–18

Jahn BM, Wu FY, Chen B (2000) Massive granitoid generation in Central Asia: Nd isotopic evidence and implication for continental growth in the Phanerozoic. Episodes 23:82–92

Jiang YH, Jin GD, Liao SY, Zhou Q, Zhao P (2010) Geochemical and Sr-Nd-Hf isotopic constraints on the origin of late Triassic granitoids from the Qinling orogen, Central China: implications for a continental arc to continent-continent collision. Lithos 117:183–197

Kelemen PB, Rilling JL, Parmentier E, Mehl L, Hacker BR (2003) Thermal structure due to solid-state flow in the mantle wedge beneath arcs. Geophys Monogr Am Geophys Union 138:293–311

Klein M, Stosch HG, Seck H, Shimizu N (2000) Experimental partitioning of high field strength and rare earth elements between clinopyroxene and garnet in andesitic to tonalitic systems. Geochim Cosmochim Acta 64:99–115

Li XH, Liu DY, Sun M, Li WX, Liang XR, Liu Y (2004) Precise Sm–Nd and U–Pb isotopic dating of the supergiant Shizhuyuan polymetallic deposit and its host granite, SE China. Geol Mag 141:225–231

Li XH, Qi CS, Liu Y, Liang XR, Tu XL, Xie LW, Yang YH (2005) Rapid separation of Hf from rock samples for isotope analysis by MC-ICPMS: a modified single-column extraction chromatography method. Geochimica 34:109–114

Li XH, Long WG, Li QL, Liu Y, Zheng YF, Yang YH, Chamberlain KR, Wan DF, Guo CH, Wang XC, Tao H (2010) Penglai zircon megacrysts: a potential new working reference material for microbeam determination of Hf–O isotopes and U–Pb age. Geostand Geoanal Res 34:117–134

Li N, Chen YJ, Fletcher IR, Zeng QT (2011) Triassic mineralization with cretaceous overprint in the Dahu Au-Mo deposit, Xiaoqinling gold province: constraints from SHRIMP monazite U-Th–Pb geochronology. Gondwana Res 20:543–552

Li T, Xu XY, Chen JL, Wang HL, Li ZP, Zhang X (2012) LA-ICP-MS zircon U-Pb dating and tectonic setting of Zhongchuan intrusion, Lixian area, west Qinling orogen. Geol Bull 31:875–883

Li XW, Mo XX, Yu XH, Ding Y, Huang XF, Wei P, He WY (2013) Petrology and geochemistry of the early Mesozoic pyroxene andesites in the Maixiu area, west Qinling, China: products of subduction or syn-collision? Lithos 172(173):158–174

Li XW, Mo XX, Huang XF, Dong GC, Yu XH, Luo MF, Liu YB (2015) U–Pb zircon geochronology, geochemical and Sr–Nd–Hf isotopic compositions of the early indosinian Tongren pluton in west Qinling: petrogenesis and geodynamic implications. J Asian Earth Sci 97:38–50

Liu SF, Steel R, Zhang GW (2005) Mesozoic sedimentary basin development and tectonic implication, northern Yangtze block, eastern China: record of continent–continent collision. J Asian Earth Sci 25:9–27

Liu SW, Li QG, Tian W, Wang ZQ, Yang PT, Wang W, Bai X, Guo RR (2011a) Petrogenesis of indosinian granitoids in middle-segment of south Qinling Tectonic Belt: constraints from Sr–Nd isotopic systematics. Acta Geol Sin Engl 85:610–628

Liu SW, Yang PT, Li QG, Wang ZQ, Zhang WY, Wang W (2011b) Indosinian granitoids and orogenic processes in the middle segment of the Qinling orogen, China. J Jilin University (Earth science edition), 41:1928-1943

Lu Z, Quan JJ, Chen X, Yan DF (2004) Characteristics and geological effects of magmatic activity of the Zhongchuan granite of western Qinling area. Acta Geologica Gan Su 12:25–30

Ludwig K (2012) User's manual for Isoplot version 3.75–4.15: a geochronological toolkit for Microsoft. Excel Berkley Geochronological Center Special Publication No. 5

Mattauer M, Matte P, Malavieille J, Tapponnier P, Maluski H, Qin XZ, Qin TY (1985) Tectonics of the Qinling belt: build-up and evolution of eastern Asia. Nature 317(6037):496–500

Martin H, Smithies RH, Rapp R, Moyen JF, Champion D (2005) An overview of adakite, tonalite–trondhjemite–granodiorite (TTG), and sanukitoid: relationships and some implications for crustal evolution. Lithos 79:1–24

Meng QR, Zhang GW (2000) Geologic framework and tectonic evolution of the Qinling-Dabie orogen, Central China. Tectonophysics 323:183–196

Mo XX, Luo ZH, Deng JF, Yu XH (2007) Granitoids and crustal growth in the east-Kunlun orogenic belt. Geol J China Univ 3:403–414 (in Chinese with English abstract)

Mo XX, Niu YL, Dong GC, Zhao ZD, Hou ZQ, Zhou S, Ke S (2008) Contribution of syncollisional felsic magmatism to continental crust growth: a case study of the Paleogene Linzizong volcanic succession in southern Tibet. Chem Geol 250:49–67

Ni ZY, Chen YJ, Li N, Zhang H (2012) Pb-Sr-Nd isotope constraints on the fluid source of the Dahu Au-Mo deposit in Qinling orogen, Central China, and implication for Triassic tectonic setting. Ore Geol Rev 46:60–67

Niu YL, O'Hara MJ (2009) MORB mantle hosts the missing Eu (Sr, Nb, Ta and Ti) in the continental crust: new perspectives on crustal growth, crust–mantle differentiation and chemical structure of oceanic upper mantle. Lithos 112:1–17

Niu YL, Zhao ZD, Zhu DC, Mo XX (2013) Continental collision zones are primary sites for net continental crust growth–a testable hypothesis. Earth Sci Rev 127:96–110

Ou CS, Yang YC, Wang H, Yang WG (2010) Characteristics and mineralization of Luchuba granite pluton in Lixian. Gansu Science and Technology 017:37–41

Peng X (2012) Magmatic consanguinity and tectonic significance of Zhongchuan rock group in western Qinling. MSc thesis, Chang'an University

Peng X (2013) Research on homology for the rock group of monzonite granite in the western Qinling. Northwest Geol 1:63–80

Pertermann M, Hirschmann MM, Hametner K, Günther D, Schmidt MW (2004) Experimental determination of trace element partitioning between garnet and silica-rich liquid during anhydrous partial melting of MORB-like eclogite. Geochem Geophy Geosy 5:297–391

Qin JF, Lai SC, Grapes R, Diwu CR, Ju YJ, Li YF (2009) Geochemical evidence for origin of magma mixing for the Triassic monzonitic granite and its enclaves at Mishuling in the Qinling orogen (Central China). Lithos 112:259–276

Qin JF, Lai SC, Grapes R, Diwu CR, Ju YJ, Li YF (2010) Origin of late Triassic high Mg adakitic granitoid rocks from the Dongjiangkou area, Qinling orogen, Central China implications for subduction of continental crust. Lithos 120:347–367

Raczek I, Jochum KP, Hofmann AW (2003) Neodymium and strontium isotope data for USGS reference materials BCR-1, BCR-2, BHVO-1, BHVO-2, AGV-1, AGV-2, GSP-1, GSP-2 and eight MPI-DING reference glasses. Geostand Newslett 27:173–179

Ratschbacher L, Hacker BR, Calvert A, Webb LE, Crimmer JC, McWilliams MO, Ireland T, Dong S, Hu J (2003) Tectonics of the Qinling (Central China): tectonostratigraphy, geochronology, and deformation history. Tectonophysics 366:1–53

Rubatto D, Gebauer D (2000) Use of cathodoluminescence for U–Pb zircon dating by ion microprobe: some examples from the western alps. In: Pagel M, Barbin V, Blanc P, Ohnenstetter D (eds) Cathodoluminescence in geosciences. Springer, Berlin, pp 373–400

Rudnick RL, Gao S (2003) Composition of the continental crust. Treatise Geochem 3:1–64

Rushmer T (1991) Partial melting of two amphibolites: contrasting experimental results under fluid absent conditions. Contrib Mineral Petrol 107:41–59

Schnetzler CC, Philpotts JA (1970) Partition coefficients of rare-earth elements between igneous matrix material and rock-forming mineral phenocrysts; II. Geochim Cosmochim Acta 34:331–340

Shen J, Zhang ZQ, Liu DY (1997) Sm–Nd, Rb–Sr, ^{40}Ar/^{39}Ar, ^{207}Pb/^{206}Pb age of the Douling metamorphic complex from eastern Qinling orogenic belt. Acta Geol Sin 18:248–254

Song SG, Niu YL, Wei CJ, Ji JQ, Su L (2010a) Metamorphism, anatexis, zircon ages and tectonic evolution of the Gongshan block in the northern Indochina continent—an eastern extension of the Lhasa block. Lithos 120:327–346

Song SG, Su L, Li XH, Zhang GB, Niu YL, Zhang LF (2010b) Tracing the 850-Ma continental flood basalts from a piece of subducted continental crust in the north Qaidam UHPM belt, NW China. Precambrian Res 183:805–816

Sun SS, McDonough WF (1989) Chemical and isotopic systematics of oceanic basalts: implications for mantle composition and processes. In: Saunders AD, Norry MJ (eds), magmatism in the ocean basins. Geol Soc London Spec Publ 42:313–345

Sun WD, Li SG, Chen YD, Li YJ (2002a) Timing of synorogenic granitoids in the south Qinling, Central China: constraints on the evolution of the Qinling–Dabie orogenic belt. J Geol 110:457–468

Sun WD, Li SG, Sun Y, Zhang GW, Li Q (2002b) Mid-Paleozoic collision in the north Qinling: Sm–Nd, Rb–Sr and ^{40}Ar/^{39}Ar ages and their tectonic implications. J Asian Earth Sci 21:69–76

Vervoort JD, Patchett PJ, Blichert-Toft J, Albarède F (1999) Relationships between Lu-Hf and Sm-Nd isotopic systems in the global sedimentary system. Earth Planet Sci Lett 168:79–99

Vervoort JD, Plank T, Prytulak J (2011) The Hf-Nd isotopic composition of marine sediments. Geochim Cosmochim Acta 75:5903–5926

Wall VJ, Clemens JD, Clarke DB (1987) Models for granitoid evolution and source compositions. J Geol 95:731–749

Wang F, Lu XX, Lo CH, Wu FY, He HY, Yang LK, Zhu RX (2007) Post-collisional, potassic monzonite–minette complex (Shahewan) in the Qinling Mountains (Central China): ^{40}Ar/^{39}Ar thermochronology, petrogenesis, and implications for the dynamic setting of the Qinling orogen. J Asian Earth Sci 31:153–166

Wang ZQ, Yan QR, Yan Z, Wang T, Jiang CF, Gao LD, Liu P (2009) The new division of the main tectonic unit for the Qinling orogenic belt. J Geol 83:1527–1546

Wang XX, Wang T, Castro A, Pedreira R, Lu XX, Xiao QH (2011) Triassic granitoids of the Qinling orogen, Central China: genetic relationship of enclaves and rapakivi-textured rocks. Lithos 2011: 369–387

Wang YL, Zhang CQ, Wang CH, Hou KJ (2012) Hf isotopic composition of the Qinjia granites from the Debao Cu deposit, Guangxi: implications for crust - mantle interaction. Geotecton Metallog 36:377–383

Wang XX, Wang T, Zhang CL (2015) Granitoid magmatism in the Qinling orogen, Central China and its bearing on orogenic evolution. Sci China Earth Sci 58:1497–1512

Wei GJ, Liang XR, Li XH, Liu Y (2002) Precise measurement of Sr isotopic composition of liquid and solid base using (LP) MC-ICPMS. Geochimica 31:295–305

Whalen JB(1985) Geochemistry of an Island-Arc Plutonic Suite: the Uasilau-Yau Yau Intrusive Complex, New Britain, P.N.G. J Petrol 26:603-632

Wiedenbeck M, Alle P, Corfu F et al (1995) Three natural zircon standards for U-Th-Pb, Lu-Hf, trace element and REE analyses. Geostandards Newslett 19:1–23

Wu YB, Zheng YF (2012) Tectonic evolution of a composite collision orogen: an overview on the Qinling–Tongbai–Hong'an–Dabie–Sulu orogenic belt in Central China. Gondwana Res 23:1402–1428

Wu FY, Jahn BM, Wilde SA, Lo CH, Yui TF, Lin Q, Ge WC, Sun DY (2003) Highly fractionated I-type granites in NE China: geochronology and petrogenesis. Lithos 66:241–273

Xiao B, Li QG, Liu SW, Wang ZQ, Yang PT, Chen JL, Xu XY (2013) Highly fractionated late Triassic I-type granites and related molybdenum mineralization in the Qinling orogenic belt: geochemical and U–Pb–Hf and Re–Os isotope constraints. Ore Geol Rev 56:220–233

Xing FM, Xu X (1996) AFC mixing model and origin of intrusive rocks from Tongling area. Acta Petrol Mineral 15:10–15

Xu JF, Castillo PR, Li XH, Zhang BR, Han YW (2002) MORB-type rocks from the paleo-Tethyan Mian-Lueyang northern ophiolite in the Qinling mountains, Central China: implications for the source of the low ^{206}Pb/^{204}Pb and high ^{143}Nd/^{144}Nd mantle component in the Indian ocean. Earth Planet Sci Lett 198:323–337

Xu XY, Li T, Chen JL, Li P (2013) The granitoids magmatism and mineralization in west section of the western Qinling, NW China. Northwest geology 5:76–82

Xu XY, Chen JL, Gao T, Li P, Li T (2014) Granitoid magmatism and tectonic evolution in northern edge of the west Qinling terrance, NW China. Acta Petrol Sin 30:371–389 (in Chinese with English abstract)

Yang JS, Wu FY, Wilde S, Liu X (2007) Petrogenesis of late Triassic granitoids and their enclaves with implications for post-collisional lithospheric thinning of the Liaodong peninsula, North China craton. Chem Geol 242:155–175

Yang PT, Liu SW, Li QG, Zhang F, Wang ZQ, Wang DS, Wang RT, Yan QR, Yan Z (2011) Ages of the Laocheng granitoids and crustal growth in the south Qinling tectonic domain, Central China: zircon U–Pb and Lu–Hf isotopic constraints. Acta Geol Sin Engl 85:854–869

Yang PT, Liu SW, Li QG, Wang ZQ, Wang RT, Wang W (2012) Geochemistry and zircon U–Pb-Hf isotopic systematics of the Ningshan granitoid batholith, middle segment of the south Qinling belt, Central China: constraints on petrogenesis and geodynamic processes. J Asian Earth Sci 61:166–186

Zeng Q, McCuaig TC, Hart CJ, Jourdan F, Muhling J, Bagas L (2012) Structural and geochronological studies on the Liba goldfield of the west Qinling orogen, Central China. Mineral Deposita 7:799–819

Zeng Q, Mccuaig TC, Tohver E, Bagas L, Lu Y (2014) Episodic Triassic magmatism in the western south Qinling orogen, Central China, and its implications. Geol J 49:402–423

Zhang GW, Zhang BR, Yuan XC, Xiao QH (2001) Qinling orogen belt and continental geodynamics. Science Press, Beijing, pp 1–729 (in Chinese)

Zhang CL, Zhang GW, Yan YX, Wang Y (2005) Origin and dynamic significance of Guangtoushan granitic plutons to the north of Mianlue zone in southern Qinling. Acta Petrol Sin 21:711–720 (in Chinese with English abstract)

Zhang HF, Jin LL, Zhang L, Nigel H, Zhou L, Hu SH, Zhang BR (2007) Geochemical and Pb-Sr-Nd isotopic compositions of granitoids from western Qinling belt: constraints on basement nature and tectonic affinity. Sci China Ser D Earth Sci 50:184–196

Zhu LM, Ding ZJ, Yao SZ, Zhang WG, Song SG, Qu WJ, Guo B, Li B (2009) Ore forming event and geodynamic setting of molybdenum deposit at Wenquan in Gansu Province, western Qinling. Chinese Sci Bull 54:2309–2324

Zhu LM, Zhang GW, Chen YJ, Ding ZJ, Guo B, Wang F, Lee B (2011) Zircon U-Pb ages and geochemistry of the Wenquan Mo-bearing granitoids in west Qinling, China: constraints on the geodynamic setting for the newly discovered Wenquan Mo deposit. Ore Geol Rev 39:46–62

Zhu LM, Zhang GW, Yang T, Wang F, Gong HJ (2013) Geochronology, petrogenesis and tectonic implications of the Zhongchuan granitic pluton in the western Qinling metallogenic belt, China. Geol J 48: 310–334